Finite Element Investigation of Cutting Performance of Cr/W-DLC/DLC Composite Coated Cutting Tool

Tianmei Hao
Qilu University of Technology
Jin Du
Qilu University of Technology
Xue Zhang (1260541626@qq.com)
Qilu University of Technology
Guosheng Su
Qilu University of Technology
Peirong Zhang
Qilu University of Technology
Yujing Sun
Qilu University of Technology
Jingjie Zhang
Qilu University of Technology
Chonghai Xu
Qilu University of Technology

Research Article

Keywords: Cr/W-DLC/DLC coating, Heat partition, Dry cutting, Finite element method

Posted Date: February 23rd, 2021

DOI: https://doi.org/10.21203/rs.3.rs-219639/v1

Finite Element Investigation of Cutting Performance of Cr/W-DLC/DLC Composite Coated Cutting Tool

Tianmei Hao, Jin Du*, Xue Zhang, Guosheng Su, Peirong Zhang, Yujing Sun, Jingjie Zhang, Chonghai Xu

School of Mechanical and Automotive Engineering, Qilu University of Technology (Shandong Academy of Sciences), Jinan, Shandong 250353, China;

*Corresponding author: Tel: +86 15853120838, E-mail:dj84105@126.com

Abstract

Coupled with a thermo-mechanical metal cutting process, rapid tool wear, higher surface roughness and mass heat are caused by the rapid plastic deformation of the workpiece and by the friction along the tool-chip interface. This phenomenon is more predominant in the machining of difficult-to-cut materials. DLC film has been applied as coating material in the machining of difficult-to-cut materials, and shows a good cutting performance. In this study, Cr/W-DLC/DLC coated tools were compared with other three coated tools (i.e., TiC-, TiAlN-, Al_2O_3-) to investigate the cutting performance in the machining of Al-Si alloy (AC9B). In addition, the influence of Cr/W-DLC/DLC coated tools on the cutting performance under different cutting speeds was studied. Cutting force, cutting temperature, heat transfer coefficient of the rake face of the tool, cutting deformation rate, plastic deformation of machined surface, the interface temperature and stress were investigated numerically based on Finite Element Method (FEM). Actual cutting experiments were carried out to the verification of the FEM models by means of the cutting force and cutting temperature measurement. The investigation results showed that Cr/W-DLC/DLC coated tools has the lowest cutting force and cutting temperature, good cutting deformation characteristics and lower coating-substrate interface temperature and stress, however appears the maximum value of heat partition coefficient into the cutting tool. With the increasing of cutting speeds, cutting force and cutting temperature showed an increase trend, while the plastic deformation depth of machined surface and heat partition into cutting tool all showed a decrease trend. This investigation can provide the theory basis or technical guidance for the cutting practice of Cr/W-DLC/DLC coated tools.

Key words: Cr/W-DLC/DLC coating; Heat partition; Dry cutting; Finite element method

1. Introduction

Advanced coating techniques have been applied on cemented carbide cutting tools in order to prolong the tool life and improve the machining quality in industrial applications[1-3]. Under the current environment protection situation, the application of conventional metal cutting with cutting fluid exhibit great limitations. Dry cutting becomes an environmental and economic machining method due to a lower friction coefficient between the coating and the work material[4]. The actual cutting experiments can obtain part of cutting performances such as cutting force, cutting temperature, machined surface roughness, and tool wear. However, some parameters during the cutting process such as the shear angle at the first deformation zone, equivalent stress, heat transfer coefficient, and temperature and stress at the tool-chip interface during the cutting process cannot be obtained. The finite element method (FEM) is a highly efficient and commonly used numerical calculation method, which has been widely used in the field of cutting. The FEM can solve the limitation of the actual cutting experiment, and the simulation result can provide more data than the experiment[5].

DLC coating began to enter the metal cutting application in the 1990s. DLC is an amorphous carbon or hydrogenated amorphous carbon thin film material which consists of graphite-like carbon within a diamond-like matrix. DLC is formed by the combination of sp^1, sp^2 and sp^3 covalent bonding coordinating carbon atoms, and a C-H covalent bond is also present in the hydrogen-containing DLC[6-8]. The sp^2 and sp^3 covalent bonding represents graphite structure and diamond structure, respectively. DLC coatings can be prepared by different deposition techniques, including Physical Vapor Deposition (PVD), Chemical Vapor Deposition (CVD) and Liquid Phase Electrodeposition. DLC film exhibits low surface roughness, high hardness, low friction coefficient, strong wear and corrosion resistance, inherently self-lubricating, and can be deposited on the cutting tools, molds, bearings, seal rings and other key components, which is an important development direction in the field of high hardness and wear-resisting coatings in the future [9-12]. DLC coating helps to improve the durability and adaptability of cutting tools, which is considered to be the strategic material in the 21st century. However, low adhesion strength between DLC film and cemented carbide tool substrate is the main obstacle for the wide application of DLC coated cutting tool, especially to single-layer DLC-coated tools[13-15]. In addition, brittle fracture is often caused

by insufficient tightness of the DLC coating when the high-speed cyclic repeated contact occurs during cutting. At present, the above problems are often solved by the addition of transition interlayers between the DLC coating and tool substrate. The roles of transition interlayer not only improve the DLC adhesion strength but also reduce the internal residual stress and improve toughness by narrowing the difference in thermal expansion coefficient, crystal structure and chemical composition mismatch between the interfaces[16].

Al-Si alloy (AC9B) is one of the cast aluminum alloys which have good casting performance, wear resistance, and the most varieties, and are widely used in the manufacture of engine pistons and other parts. The Al-Si alloy (AC9B) has poor machinability, and the small chips generated during the cutting process may scratch the machined surface which leading to poor surface quality and serious tool wear. The traditional coatings like TiC、TiN、Al_2O_3 and AlN etc. have some limitations in the cutting of Al–Si alloy due to the strong adhesion, chemical reaction and severe hard particle wear. In contrast, DLC coated tools have perfectly chemical inertness and inherently self-lubricating properties, and are appropriate for the cutting of Al-Si alloys. S. Bhowmick et al. [17]used hydrogenated diamond-like carbon (α:C-H) coatings and diamond coatings for subeutectic (Al-6.-18.5% Si) aluminum alloy was drilled. The results show that aluminum adhesion is a limiting factor for performance when drilling aluminum-silicon alloys, and α:C-H coated tools can replace CVD diamond coated tools. A. D'Orazio[18] and A, Maksym Ziberov[19] used DLC coated tools and TiAlN coated tools to process AA7075 alloy and Ti-6Al-4V alloy respectively. The results show that the wear of DLC coated tools is lower than that of TiAlN coated tools.

Considering the potential application of DLC composite coated tools in cutting Al-Si alloys, whole DLC coated cemented carbide tools were prepared by direct current plasma enhanced chemical vapor deposition (PACVD). The coating deposited by PACVD technology has compact structure, small roughness and can be deposited at low temperature[20]. In this investigation, YG8 (WC 92%, Co 8%) cemented carbide tool was chosen to be the substrate, Cr/W-DLC/DLC composite coatings was chosen to be the coating. HauTer Coater (HC-1500) coating equipment was employed to prepare Cr/W-DLC/DLC composite coating. The magnetron sputtering process prepares the Cr and W-DLC interlayer, and the plasma enhanced chemical vapor deposition process prepares the outermost layer of DLC. Cr as the first transition interlayer can be attributed to three reasons. First, Cr, as a transition element, has higher hardness, higher density, good ductility, electrical

conductivity and thermal conductivity. Second, it can block the adverse effect of Co element in the carbide matrix on the nucleation of carbon atoms. Finally, Cr, as a carbide-forming element, can enter part of the solid solution in an atomic state, another form a displacement alloy cementite, and some form a bonding phase with the cemented carbide substrate to form an alloy-phase bonding interface that can be well combined with the cemented carbide matrix[21]. The second transition interlayer is a DLC coating doped with W element. The doped W element will exist as an amorphous structure in the carbon network structure, thereby alleviating internal residual stress (reducing pressure concentration) and enhancing comprehensive performance. As a support layer, increase the crack suppression rate and increase the elastic recovery rate. The thicknesses of Cr/W-DLC/DLC composite coatings was-3.3 μm. Cross-sectional morphology of Cr/W-DLC/DLC composite coating with transition interlayers on YG8 cemented carbide substrate were observed as shown in Fig. 1(a), The EDS spectral line scanning area is indicated by the arrowed line in the cross-sectional morphology of Fig. 1(a), and the arrow direction indicates the EDS spectrum line scanning direction. It can be seen from Fig. 1(b), in addition to the substrate elements W and Co, the coating region also contains Cr, W and C elements. It can be obviously seen that the content of each element in the Cr/W-DLC/DLC composite coating is apparently distributed. It is confirmed that Fig. 1(b) is a Cr/W-DLC/DLC composite coating.

In this study, the numerical simulation software AdvantEdge is employed to investigate the cutting performance of Cr/W-DLC/DLC composite coating tools in the machiningof Al-Si alloy (AC9B). The influence of coating materials (TiC-, TiAlN-, Al_2O_3-, Cr/W-DLC/DLC-) and cutting speeds on cutting performance was discussed. The cutting performances of Cr/W-DLC/DLC coated tools in cutting force, cutting temperature, cutting deformation, heat conductivity were studied. In addition, the influence of cutting speed on the above properties was also studied. The results can contribute to the further study of Cr/W-DLC/DLC- coated tool failure mechanism and tool life. The description of the experiment methodology flow chart is shown in Fig. 2.

Therefore, the research in this paper provides a basis for the development of DLC composite coatings and provides a basis for the application of DLC composite coatings in the field of cutting.

2. Validation of cutting simulation FEM model

2.1 Validation of orthogonal cutting FEM model

The ambient temperature of workpiece and cutting tool is set to 20°C. The length of workpiece

is 6mm and the height is 2mm. In the cutting simulation, the cutting tool is fixed in the X and Y directions, and the workpiece is set to move in the X positive direction with the cutting speed relative to the tool, while the Y direction is fixed. The tool cuts into the workpiece from the initial position. The chips continue to formation as the tool cuts in. The friction coefficient between DLC coated cemented carbide tool and high Al-Si alloy as 0.1[22]. The simulation calculation model selects the standard detailed calculation (Standard) mode. Metal cutting can be regarded as a process where large deformations are highly concentrated in a small region[23].The 3-D cutting simulation cutting model is converted into a 2-D cutting simulation model to reduce the simulation time without affecting the results, as shown in Fig. 3.As shown in Fig. 3, the element topology used is a 6-noded quadratic triangle element with three corners and three midsize nodes. The initial mesh becomes distorted after a certain cut length, and it will be remeshed in this vicinity to form a regular mesh again. In this study, the mesh of the tool tip and cutting deformation area are appropriately encrypted, and other parts are divided by a larger mesh. The maximum and minimum dimensions of the tool mesh unit are 0.1mm and 0.02mm, respectively. The mesh division parameter is set to 0.4.

2.2 Validation of material constitutive FEM model

The workpiece material is subjected to high temperature, large strain, and large strain rate then will occurs thermo-elastic plastic deformation during metal cutting. Therefore, the selection of the correct constitutive model is the basis and prerequisite to ensure the correctness and reliability of the dynamic physical simulation results of the machining process. The software built-in constitutive model of workpiece material is the Power Law material constitutive model (power exponential material model) which comes with the AE software constitutive equation library and employed before the simulation. The constitutive equation is as follows:

$$\sigma(\varepsilon^{p},\dot{\varepsilon},T)=g(\varepsilon^{p})*\Gamma(\dot{\varepsilon})*\Theta(T) \quad (1)$$

Where $g(\varepsilon^{p})$ is the strain strengthening function, $\Gamma(\dot{\varepsilon})$ is the strain rate effect function, and $\Theta(T)$ is the thermal softening function. The thermo-physical properties of the workpiece material (AC9B) are shown in Table 1. The YG series is selected as the tool substrate material which corresponding to Carbide Grade K in the tool library of the AdvantEdge software. The coating materials are customization and designed as Cr/W-DLC/ DLC. The simulation parameters of each interlayer materials are shown in Table 2.

2.3 Heat conduction model at tool rake face

As all known, there are three deformation zones which generate cutting heat during the cutting process. Shaw[24] proposed that all the cutting energy transfers into heat during the cutting process. The heat conducts into the workpiece, cutting tool, and chip as shown in Fig. 4. In the secondary deformation zone, the proportion of cutting heat flowing into the chip at the tool-chip interface can be represented by the symbol R_2. R_2 is called the chip heat distribution coefficient. Using the measurement tool from Advantedge FEM to measure the shear angle and chip thickness at the same simulation step is shown in Fig. 5. The l_f is the tool-chip contact length along the rake face of the tool. With reference to the slip line theory proposed by Lee and Shaffer[25], l_f can be determined by the formula shows in (1).

$$l_f = h_D \frac{\sqrt{2}}{2\sin\phi\sin(\frac{\pi}{4}+\phi-\gamma_0)} \qquad (2)$$

Where h_D is the under-formed chip thickness, ϕ is the shear angle, and γ_0 is the tool rake angle.

The effective heat distribution coefficient (R_2) entering to the chip at the tool-chip interface is described as follows[26].

$$R_2 = \frac{q_2(l_f \overline{A}/k_1) - \overline{\theta_s} + \theta_0}{q_2(l_f \overline{A}/k_1) + q_2(0.377 l_f / k_2\sqrt{v_{ch} l_f / 4\alpha})} \qquad (3)$$

Where q_2 is the heat flux in the secondary deformation zone, $\overline{A}$ is the shape factor, k_1 is the thermal conductivity of tool, $\overline{\theta_s}$ is the mean temperature nearby the first deformation zone, θ_0 is the ambient temperature of workpiece, k_2 is the thermal conductivity of chip, v_{ch} is the Chip velocity, and α is the thermal diffusivity of workpiece.

Thus, heat partition coefficient into the cutting tool (R_{tool}) is represented as follows:

$$R_{tool} = 1 - R_2 = 1 - \frac{q_2(l_f \overline{A}/k_1) - \overline{\theta_s} + \theta_0}{q_2(l_f \overline{A}/k_1) + q_2(0.377 l_f / k_2\sqrt{v_{ch} l_f / 4\alpha})} \qquad (4)$$

3. Verification of the FE models by means of the cutting force and temperature measurement

For the validation of the FEM model, actual cutting experiments were carried out and then, the cutting forces and cutting temperatures were measured. Cutting tools had 20° rake angle and

0°clearance angle and 0.5mm cutting edge radius. The cutting speeds employed in this experiment were 78, 152, 244, 304, and 378m/min. Depth of cut and feed rate were maintained constants at 0.4 mm and 0.1 mm/r, respectively. All of the cutting tests were conducted at a lathe CA6140 (maximum speed 1400r/min, power 7.5KW). The experiment set up is exhibited in Fig. 6. Advanced infrared thermal imager FLIR A315 was employed to record the cutting temperature during the cutting process. Infrared thermal imager has been calibrated according to calibration specification for thermal images-JJF 1187-2008. A Kistler 9129A dynamometer was adopted to measure the three direction of cutting forces (F_x/F_y/F_z).

The change of main cutting force and cutting temperature obtained by dynamometer and simulation are shown in Fig. 7 and Fig. 8, respectively. Fig. 7 shows the resultant cutting force comparison measured from Cr/W-DLC/DLC coated tools through cutting experiments and FE simulations. As can be seen from Fig. 7, the simulated cutting force test values of Cr/W-DLC/DLC coated tools at different speeds are basically the same as the test values with the actual cutting process. The influences of cutting speeds on the cutting temperature obtained by cutting experiments and simulations are presented in Fig. 8. As can be seen from Fig. 8, the influence of cutting speeds on cutting temperature of Cr/W-DLC/DLC coated tools obtained by FEM simulations is similar to the experimental value, and the cutting temperature increases with the increase of cutting speed.

The simulation process is established under certain assumptions and theoretical conditions. The constitutive model and material parameter settings used are different from the actual workpiece material. In addition, there is a gap between chip fracture and separation criteria with the actual cutting, which makes the gap between simulation results and the actual cutting situation reasonable. Therefore, the finite element model was verified by measuring the main cutting force and cutting temperature in actual cutting experiments. It can be verified by Fig. 7 and Fig. 8 that the finite element model can be used to analyze the cutting performance of coated tools.

4. Influences of coating materials on cutting performance

Elastoplastic deformation and friction occur in the cutting tools, chips and the surface layer of the workpiece during metal cutting, which will generate cutting force and cutting heat. Cutting force and cutting heat directly affect tool wear and durability, machining accuracy and machined surface quality. Cutting heat is mainly transmitted by chips, workpieces, cutting tools and surrounding media. The main factors affecting cutting heat conduction are as follows: heat conduction of workpiece

material, heat conduction of tool material, surrounding medium, contact time between chip and tool. The cutting parameters are v_c = 400m / min, a_p= 2mm, f = 0.15mm/r, and the cutting length is 5mm.

4.1 Influences of coating materials on cutting temperature and cutting force

TiC coating has higher hardness, strength and stiffness, and has a lower coefficient of friction (about 0.2 -0.3)[27]. At the same time, it has good thermal stability (melting point above 3000℃) and good electrical conductivity[28]. Al_2O_3 coating has excellent heat resistance and stability[29]. TiAlN coating has good high temperature oxidation resistance and age hardening[30]. At present, these materials have been widely used in high-temperature and wear-resistant coatings in cemented carbide tools in dry cutting. Al_2O_3, TiAlN, and TiC coating materials were selected as comparisons to study the performance of Cr/W-DLC/DLC coated tools in cutting force, cutting temperature, cutting deformation, coating-substrate interfacial stress, and thermal conductivity of the rake face.

Fig. 9 shows a comparison of various cutting forces measured by finite element simulations from TiC, TiAlN, Al_2O_3, and Cr/W-DLC/DLC coated tools. In Fig. 9(a), F_x and F_y are the cutting component forces in the x and y directions, respectively, and F is the total cutting force; F_f is the tangential frictional force acting on the rake face of the chip; F_n is the normal force of the chip acting on the rake face, and γ_0 is the rake angle of the tool. Then there are:

$$\mathrm{F} = \sqrt{{F_x}^2 + {F_y}^2} \tag{5}$$

$$F_f = F_x sin\gamma_0 + F_y cos\gamma_0 \tag{6}$$

$$F_n = \sqrt{F^2 - {F_f}^2} \tag{7}$$

where F_x and F_y are average values of stable cutting. In this way, the total cutting force, tool-chip friction force and normal force of different coated tools are obtained. As shown in Fig. 9(a), various cutting forces measured during cutting process of Cr/W-DLC/DLC coated tools are significantly smaller than other coated tools. The main reason for the difference in cutting force is the different friction coefficient between the coating material and the workpiece material (Al-Si alloy AC9B). The Cr/W-DLC/DLC coating has self-lubricating property, so the friction coefficient of Cr/W-DLC/DLC coating tool and Al-Si alloy is significantly smaller than that of other three coated tools. The smaller of the tool-workpiece friction coefficient means that the lower friction and the lower energy consumption. The change of cutting temperature with the cutting distance from the finite element analysis is shown in Fig. 9(b). The cutting peak temperature of the four coated tools is $A1_2O_3$>

TiA1N>TiC >Cr/W-DLC/DLC. The thermal conductivity parameters of the four coating materials are shown in table 3[26, 31-33].

4.2 Influences of coating material on shear angle and chip thickness

Shear angle and chip thickness are important parameters that can be employed to evaluate the cutting deformation[26]. As shown in Fig.10, the four kinds of coated tools have different chip thicknesses and shear angles under the same cutting conditions. A larger shear angle and a smaller chip thickness mean a lower cutting deformation rate, which indicates a relatively small deformation in the cutting deformation area. It can be seen from Fig. 10 that the Cr/W-DLC/DLC coated tool has the smallest chip thickness and the largest shear angle, which means that the Cr/W-DLC/DLC coated tool undergoes minimal deformation during processing. According to metal cutting principle[24], cutting deformation ration (Δh) can be defined as the following equation:

$$\Delta h = \cot\phi\cos\gamma_0 + \sin\gamma_0 \tag{5.13}$$

where ϕ is the shear angle in the first deformation zone. The cutting deformation rate obtained from the cutting deformation ration equation is shown in Fig.11. It further intuitively verified the cutting deformation ration of four kinds of coated tools for cutting Al-Si alloy (AC9B). It can be seen that the cutting deformation corresponding to the TiC coated tool is the largest one while the Cr/W-DLC/DLC coated tool is the smallest one.

4.3 Influences of coating materials on heat distribution

An infrared thermal imager can be used to measure the real-time temperature of the whole cutting zone in the actual cutting test. However, the temperature distribution of the rake face of the cutting tool cannot be distinguished, including the location of the peak temperature and the peak temperature of the rake face. Therefore, the thermal conductivity in the coating material of cutting tool and the temperature field of cutting tool substrate which can't be clearly obtained by infrared thermal imager while can be obtained by using finite element analysis. The average value of the temperature of the cutting deformation zone was recorded as the simulation result of the cutting temperature.

The temperature distribution in the tool can also be clearly seen from Fig. 12. Based on these temperature clouds, not only the maximum temperature on the rake face of the tool can be determined, but also the temperature distribution perpendicular to the rake face of the tool can be

obtained. It can be seen from Fig. 12 that the chip temperature gradient is large, and it can be seen that most of the cutting heat is taken away by the chip. The Cutting temperature field shown in Fig. 12 can be used to study the effect of tool coating materials on the maximum temperature. In the same temperature range, the distribution area and temperature value of Al_2O_3 coated tools in the high temperature area are significantly higher than those of TiAlN coated tools and TiC coated tools. The temperature distribution of Cr/W-DLC/DLC coated tools is shown in Fig. 12(d). It can be seen that the highest temperature on the rake face is significantly lower than the other three coatings, and the area size of the high temperature area is also significantly lower than the other three coated tools. This shows that the thermal diffusion effect of Cr/W-DLC/DLC coated tools is significantly better than the other three coating materials.

The position of the peak temperature on the tool rake face is determined by the tool-chip contact length, which can be defined as Eq. (2). According to Eq. (2), the tool-chip contact length is defined by the cutting depth, cutting angle and tool rake angle. The shear angle is the determining factor when the cutting depth and tool rake angle are constant. Therefore, as the shear angle increases, the contact length between the tool and the chip decreases. It can be inferred that as the shear angle decreases, the value of the peak temperature position of the tool rake face increases. It can be seen from Fig. 10 that the four coating materials have four different shear angles when cutting Al-Si alloy (AC9B). Compared with TiAlN and TiC coated tools, Al_2O_3 has the largest shear angle. Therefore, it can be inferred Al_2O_3 coated tools have the shortest chip contact length on the rake face of the tool that compared with TiAlN and TiC coated tools. Cr/W-DLC/DLC coated tools have the largest shear angle and the location of peak temperature is closest to the tool tip compared with other three coating tools.

Fig. 13 shows the peak temperature of the rake face and their location of the four coated tools obtained at the same coating thickness (coating thickness of 3.3μm) and the same cutting speed (cutting speed of 400m/min). As shown in Fig. 13, the coordinates on the left represent the peak temperature of the rake face, and the coordinates on the right represent peak temperature location of the tool rake face, that is, the distance (l) from the tip to the peak temperature position on the tool rake face. The distance (l) from the tip to the peak temperature location is indicate in Fig. 5. As shown in Fig. 13, the Al_2O_3 coated tool has the highest rake face temperature among the four coated tools but the peak temperature location on the rake surface is the shortest. Cr/W-DLC/DLC coated

tools have a minimum rake face temperature of 189.3℃, and the highest temperature of the rake face is the shortest distance from the tool tip, about 24.22μm. Fig.14 shows the change of the horizontal distance between the temperature values of different coated tools and the peak temperature of rake face. It can be seen from the figure that the temperature of the four coated tools at the highest point of the rake face decreases approximately linearly with the increase of the horizontal distance. The temperature of Cr/W-DLC/DLC coated tools decreased slowly with a small slope. The results show that Cr/W-DLC/DLC coated tool has a gentle temperature change and a small thermal impact to the substrate, which can protect the substrate material better.

The proportion of heat transferred to the cutting tool mainly depends on the thermal conductivity of the coating material. For the steady-state heat conduction of coated tools, the smaller the thermal conductivity of the coating material of the tool, the less heat is conducted to the tool. Thus, the lower the temperature of the coated tool substrate. Comparing the thermal conductivity of the four coatings, Cr/W-DLC/DLC>TiC>TiAlN>Al_2O_3. According to the simulation results, combined with the characteristics of the workpiece and the coating material, the heat distribution of the tool can be calculated according to Eq. (4), as shown in Fig. 15. Fig. 15 shows the heat distribution coefficients of TiC-, TiAlN-, Al_2O_3- and Cr/W-DLC/DLC- coated tools under the same cutting conditions (400m/min cutting speed). Among these four coatings, the heat distribution of the Cr/W-DLC/DLC coated tool of the rake face in the cutting tool is the maximum (R_{tool} = 0.17), and the heat distribution of the Al_2O_3 coated tool in the cutting tool is the minimum (R_{tool} = 0.031). Among them, compared with the heat distribution rate of TiC-, TiAlN-, Al_2O_3 -coated tools, the heat distribution coefficient of TiC coated tools is the largest, (R_{tool} = 0.064). This is because the thermal conductivity of the TiC coating material is larger than that of the TiAlN and Al_2O_3 coating materials, so the temperature proportion to the tool is high, the heat transfer effect is obvious, and the tool temperature is high. Compared with TiAlN and Al_2O_3, the thermal barrier effect of TiC coating material on cutting heat conduction during cutting is weakened. The Al_2O_3 coating has the characteristics of low thermal conductivity which can effectively prevent cutting heat from flowing into the tool during the cutting process and suppressing the increase of the tool temperature. The thermal conductivity of the Cr/W-DLC/DLC coating is 500W•m^{-1}•K^{-1} that much higher than the other three coatings. The high thermal conductivity of Cr/W-DLC/DLC coating means that it provides the highest heat distribution rate for cutting tools in the tool-chip interface. According to Fig.

9(b), Cr/W-DLC/DLC coated tools generate much less cutting heat in the cutting process than the other three coated tools. It can be inferred that although the large thermal conductivity of the Cr/W-DLC/DLC coating results in a large heat distribution coefficient that is conducted into the tool, but the cutting heat of the tool entering Cr/W-DLC/DLC coating is far less than the other three coating tools in the actual cutting process.

4.4 Influences of coating materials on the temperature and stress of coating-substrate interface

The temperature and stress at the coating-substrate interface have an important effect on the failure of the coating. Too high temperature at the coating-substrate interface will deform the matrix of the substrate or the coating. Too high stress will cause the coating to peel off and fail**.** Therefore, it is important to study the temperature and stress at the coating-substrate interface. The temperature and stress values at the coating-substrate interface of TiC-, TiAlN-, Al_2O_3- and Cr/W-DLC/DLC-coated tools are shown in Fig. 16. It can be seen from Fig. 16 that the temperature and stress values at the coating-substrate interface of the Al_2O_3 coated tool are the highest, which are 293.82℃ and 440.473MPa, respectively. Cr/W-DLC/DLC coated tools have the lowest temperature and stress values at the coating-substrate interface, which are 184.954℃ and 346.51MPa, respectively.

It is divided into two parts near the stagnation point on the fillet of the tool tip when metal is cutting. One part of the metal is pressed into the chip, and the other part is pressed into the new working surface. The metal layer pressed into the chip swells near the rake face of the tool, which helps the chip to curl. Metals that are pressed into a newly produced machined surface usually have residual stress after machining. Fig. 16(b) shows the distribution of the equivalent stress along the maximum value of the tip toward the inside of the tool in the rake surface about coated tool. The extension direction is shown in Fig. 16(a). It can be seen from Fig. 16(b) that the stress value and stress gradient in the coated tool change greatly, and the stress suddenly changes at the interface between the coating and the substrate. It will cause cracking and peeling of the coating material at the interface when the equivalent stress exceeds a certain value. Fig. 17 and Fig. 18 shows the equivalent stress distribution and enlarged view of the rake face and flank face during the simulation. It can be seen from Fig. 17 that the stress reaches a maximum at a certain distance from the flank face to the tool tip, which corresponds to the position where the flank face wear occurs.

5. Influences of cutting speed on cutting performance

In the finite element simulation of Cr/W-DLC/DLC coated tools, five cutting speeds were used,

namely v_c = 400, 800, 1200, 1600, 2000m/min, a_p = 2mm, f = 0.15mm/r, the simulated cutting length is 5mm.

5.1 Influences of cutting speed on cutting temperature and cutting force

The friction force between the cutting tool and the workpiece material in the secondary deformation zone and the tertiary deformation zone are increases as the cutting speed increases. On the one hand, an increase in tool-workpiece friction force results in an increase in cutting force. On the other hand, faster cutting speed will cause rapid plastic deformation and shear slip in the main cutting deformation area. This rapid deformation and shear slip will also lead to the increase of cutting force. The increase of cutting force and friction force leads to the increase of cutting temperature. Fig. 19 and Fig. 20 show the cutting force and cutting temperature corresponding to different cutting speeds. It can be seen from Fig. 19 and Fig. 20 that both the cutting force and the cutting temperature increase with the increasing of the cutting speed.

5.2 Influences of cutting speed on shear angle and chip thickness

After simulation, the shear angle and chip thickness are measured, as shown in Fig. 21. The results show that with the increase of cutting speed, the shear angle increases, while the chip thickness decreases. In other words, higher cutting speed will cause smaller deformation in the cutting process. The results of Fig. 22 also prove the relationship between cutting speed and cutting deformation on the other hand. It can be seen from Fig. 22 that the cutting deformation ration and the tool-chip contact length decrease with the increase of cutting speed.

5.3 Influences of cutting speed on plastic deformation of machined surface

There are two reasons for the plastic deformation of the machined surface. On the one hand, there will be negative shear zone below the cutting layer in front of the tool tip in the process of cutting. In the negative shear region, the workpiece material will produce plastic shear slip and bending deformation, which results in plastic deformation of the machined surface. On the other hand, friction occurs between the flank face of the tool and the machined surface in the third deformation zone which will result in residual stress and work hardening on the machined surface. The surface plastic deformation after cutting is an important factor that affecting the surface integrity and mechanical properties of the machined workpiece. The high plastic deformation of the machined surface will cause high residual stress and change the grain structure, which will affect the fatigue strength and fatigue life of the workpiece. The plastic deformation value of the machined surface

decreases with the increase of the depth of the material from the machined surface in the vertical direction[34]. The cutting parameters in the cutting process are one of the factors that affect the plastic deformation of the machined surface. Fig. 23 shows the depth of plastic deformation at different cutting speeds. The schematic diagram of plastic deformation depth measurement is shown in Fig. 23 (a). It can be seen that the cutting speed has a great influence on the thickness of the plastic deformation of the machined surface from the values in Fig. 23 (b). The increase of cutting speed will reduce the thickness of the plastic deformation layer on the machined surface when other cutting parameters remain unchanged. The maximum plastic deformation depth of the machined surface is 0.16mm when the cutting speed is 400m/min. The plastic deformation depth of the machined surface is reduced to 0.05mm when the cutting speed is 2000m/min. This is due to the contact time between the tool and the workpiece material decreases with the increase of the cutting speed, and the contact time between the two materials are not enough to support the plastic deformation of the machined surface of the workpiece material.

5.4 Influences of cutting speed on heat distribution

The temperature of the secondary deformation zone is mainly produced by the friction between the tool and chip during the cutting process. With the increase of friction time, the friction heat is accumulated from the tip point along the rake face of the tool. The temperature accumulation reaches the maximum value when moving to the chip separation point. The separation point is the highest temperature position of the rake face about tools. It can be seen from Fig.24 that the temperature of the rake face increases with the increase of cutting speed, and the distance between the highest temperature of the rake face and the tool tip decreases with the increase of cutting speed. This shows from the side that the tool chip contact length decreases with the increase of cutting speed. The tool chip contact length directly affects the friction in the cutting process, and then affects the chip deformation ration, machined surface integrity and tool wear. It can be concluded that the higher the speed, the more conducive to the cutting process under the same cutting feed and cutting depth parameters.

Five cutting speeds were employed through FE simulation to study the influence of cutting speeds on the heat partition into cutting tool in the tool-chip interface. The influence of cutting speeds on the heat partition into cutting tool is shown in Fig. 25. It is illustrated in Fig. 25 that heat partition coefficient shows a reduce trend whole as the increasing of cutting speeds. That means

higher cutting speed induces less heat entering to cutting tool in tool-chip interface. When the cutting speed ranges from 400 to 800m/min, the heat partition coefficient varies from 0.17 down to 0.11. The change trend of heat distribution coefficient becomes slower when the cutting speed is more than 800m/min, which indicates that the change of heat distribution coefficient of conduction into tool is very small. As all known, on the one hand, faster cutting speed that induces the tool-chip contact time is shortened and then cutting heat has relatively less time flowing into cutting tool. On the other hand, a mass of cutting heat generated at secondary deformation zone is carried away by high-speed chip with the increasing of cutting speeds. Therefore, cutting heat generated in secondary deformation zone partition into tool reduces as the increasing of cutting speeds.

6 .Conclusions

Cutting performance including cutting force, cutting temperature, cutting deformation rate, coating-substrate interface temperature and stress, and heat partition into cutting tool was investigated in the machining of Al-Si alloy (AC9B) with coated tools. The influences of Cr/W-DLC /DLC coated tools on the cutting performance were studied and compared with other coated tools based on FE simulations and cutting experiments. The main conclusions are as follows:

(1).The results of Cr/W-DLC/DLC coated tools are in good agreement with the cutting force and cutting temperature obtained from the FE simulations and cutting experiments. That is to say, this FE model can be used to the analysis of coated tool cutting performance. It can be employed to obtain the cutting parameters which cannot be obtained by the actual cutting experiments.

(2).The cutting force and cutting temperature in the cutting process of Cr/W-DLC/DLC coated tools are significantly lower than those of the TiC-, TiAlN-, Al_2O_3- coated tools due to the Cr/W-DLC/DLC coating has self-lubricating characteristics and low coefficient of friction. Cr/W-DLC/DLC coated tools have higher thermal conductivity than composite coatings, and the calculated heat distribution coefficient is higher than TiC-, TiAlN-, Al_2O_3- coated tools.Cr/W-DLC /DLC coated tools also have good cutting deformation characteristics, lower film-based interface temperature and stress, which is beneficial to actual cutting processing.

(3).Cr/W-DLC/DLC -coated tool has the minimum rake face temperature and the peak temperature location on the rake face distance from the tool tip among the four coated tools;.

(4).With the increase of cutting speed, the cutting force and temperature gradually increased, the cutting deformation rate, the depth of plastic deformation of the machined surface and the thermal

conductivity of the rake surface gradually decreased.

Acknowledgments

This work was supported by the National Natural Science Foundation of China (51675289,51905286), Natural Science Foundation of Shandong province(ZR2020ME160), Key research and development plan of Shandong Province (2019GGX104052) ,Project for the Innovation Team of Universities and Institutes in Jinan(2018CXRC005).

References

1. Cui X, Zhao J (2014) Cutting performance of coated carbide tools in high-speed face milling of AISI H13 hardened steel. International Journal of Advanced Manufacturing Technology 71:1811-1824. https://doi.org/10.1007/s00170-014-5611-3
2. Chinchanikar S, Choudhury SK (2015) Cutting force modeling considering tool wear effect during turning of hardened AISI 4340 alloy steel using multi-layer TiCN/Al_2O_3/TiN-coated carbide tools. International Journal of Advanced Manufacturing Technology 83:9-12. https://doi.org/10.1007/s00170-015-7662-5
3. Yan S, Zhu D, Zhuang K, Zhang X, Ding H (2014) Modeling and analysis of coated tool temperature variation in dry milling of Inconel 718 turbine blade considering flank wear effect. Journal of Materials Processing Tech 214:2985-3001. https://doi.org/10.1016/j.jmatprotec.2014.07.006
4. Heaney PJ, Sumant AV, Torres CD, Carpick RW, Pfefferkorn FE (2008) Diamond coatings for micro end mills: enabling the dry machining of aluminum at the micro-scale. Diamond and Related Materials 17:223-233. https://doi.org/10.1016/j.diamond.2007.12.009
5. Jafarian F, Ciaran MI, Umbrello D, Arrazola P, Filice L, Amirabadi H (2014) Finite element simulation of machining Inconel 718 alloy including microstructure changes. International Journal of Mechanical Sciences88:110-121. https://doi.org/10.1016/j.ijmecsci.2014.08.007
6. Ishikawa T, Choi J (2018) The effect of microstructure on the tribological properties of a-C:H films. Diamond & Related Materials 89:94-100. https://doi.org/10.1016/j.diamond.2018.08.009
7. Wei X, Zhou KS, Lin S, Dai M, Qian S, Wei C (2018) Structural properties of hydrogenated Al-doped diamond-like carbon films fabricated by a hybrid plasma system. Diamond & Related Materials 87:177-185. https://doi.org/10.1016/j.diamond.2018.06.012
8. Vetter J (2014) 60 Years of DLC coatings: Historical highlights and technical review of cathodic arc processes to synthesize various DLC types, and their evolution for industrial applications. Surface & Coatings Technology 257:218-240. https://doi.org/10.1016/j.surfcoat.2014.08.017
9. Bewilogua K, Hofmann D (2014) History of diamond-like carbon films—from first experiments to worldwide applications. Surface and Coatings Technology 242:214-225. https://doi.org/ 10.1016/j.surfcoat.2014.01.031
10. Changning B, Aimin L, Zhongyue C, Li Q, Junyan Z (2018) Achieving a high adhesion and excellent wear resistance diamond-like carbon film coated on NBR rubber by Ar plasma pretreatment. Diamond & Related Materials 89:84-93. https://doi.org/ 10.1016/j.diamond.2018.08.013
11. Fenili CP, De Souza FS, Marin G, Probst SNMH, Binder C, Klein AN (2017) Corrosion resistance of low-carbon steel modified by plasma nitriding and diamond-like carbon. Diamond & Related Materials 80:153-161. https://doi.org/10.1016/j.diamond.2017.11.001
12. Jokari-Sheshdeh M, Mahboubi F, Dehghani K (2018) Structure and tribological behavior of diamond-like carbon coatings deposited on the martensitic stainless steel: The influence of gas composition and temperature. Diamond & Related Materials 81:77-88. https://doi.org/10.1016/j.diamond.2017.11.007
13. C.W. Zou, H.J. Wang, L. Feng, S.W. Xue (2013) Effects of Cr concentrations on the microstructure, hardness, and temperature-dependent tribological properties of CrDLC

coatings. Appl. Surf. Sci. 286 :137–141. https://doi.org/10.1016/j.apsusc.2013.09.036
14. Salvadori MC, Teixeira FS, Araújo WWR, Sgubin LG, Brown IG (2012) Interface tailoring for adhesion enhancement of diamond-like carbon thin films. Diamond & Related Materials 25:8-12. https://doi.org/ 10.1016/j.diamond.2012.02.005
15. A.C., Ferrari, and, S.E., Rodil, and, J., Robertson, and, W.I. (2003) Erratum to "Is stress necessary to stabilise sp3 bonding in diamond-like carbon": [Diamond Relat. Mater. 11 (2002) 944–999]. Diamond & Related Materials12:1439-1439. https://doi.org/10.1016/S0925-9635(03)00164-X
16. Yeldose BC, Ramamoorthy B (2008) Characterization of DC magnetron sputtered diamond-like carbon (DLC) nano coating. The International Journal of Advanced Manufacturing Technology 38:705-717. https://doi.org/ 10.1007/s00170-007-1131-8
17. Bhowmick S, Banerji A, Alpas A (2015) Tribological behavior of Al–6.5%,–12%,–18.5% Si alloys during machining using CVD diamond and DLC coated tools. Surface and Coatings Technology 284:353-364. https://doi.org/ 10.1016/j.surfcoat.2015.08.073
18. A.D'Orazio, M.El, Mehtedi, A.Forcellese, A.Nardinocchi, M.Simoncini (2017) Tool wear and hole quality in drilling of CFRP/AA7075 stacks with DLC and nanocomposite TiAlN coated tools. Journal of Manufacturing Processes 30:582-592. https://doi.org/10.1016/j.jmapro.2017.10.019
19. a MZ, a DdO, a MBdS, b WNPH (2020) Wear of TiAlN and DLC coated microtools in micromilling of Ti-6Al-4V alloy. Journal of Manufacturing Processes 56:337-349. https://doi.org/10.1016/j.jmapro.2020.04.082
20. Sharifahmadian O, Mahboubi F (2019) A comparative study of microstructural and tribological properties of N-DLC/DLC double layer and single layer coatings deposited by DC-pulsed PACVD process. Ceramics International 45:7736-7742. https://doi.org/10.1016/j.ceramint.2019.01.076
21. Hong YS, Kwon SH, Wang T, Kim DI, Choi J, Kim KH (2011) Effects of Cr interlayer on mechanical and tribological properties of Cr-Al-Si-N nanocomposite coating. Transactions of Nonferrous Metals Society of China 21-21. https://doi.org/10.1016/S1003-6326(11)61062-5
22. Ronkainen H, Holmberg K (2008) Environmental and thermal effects on the tribological performance of DLC coatings. In Tribology of diamond-like carbon films. Springer US： 155-200. https://doi.org/10.1007/978-0-387-49891-1-6
23. Chen M, Ni H, Wang Z, Jiang Y (2012) Research on the modeling of burr formation process in micro-ball end milling operation on Ti–6Al–4V. The International Journal of Advanced Manufacturing Technology 62:901-912. https://doi.org/10.1007/s00170-011-3865-6
24. Shaw MC, Cookson J (2005) Metal cutting principles. Oxford university press New York
25. Lee E (1951) The theory of plasticity applied to a problem of machining. ASME J Appl Mech 18:405. https://doi.org/10.1007/BF00412000
26. Jin D, Jingjie Z, Liguo W (2018) Heat partition and rake face temperature in the machining of H13 steel with coated cutting tools. The International Journal of Advanced Manufacturing Technology 94:3691-3702. https://doi.org/10.1007/s00170-017-1122-3
27. Groning P, Nowak S, Schaller E, Schlapbach L (1993) Initial stages of titanium carbide growth by plasma-sputter deposition on stainless steel. Applied Surface Science(The Netherlands) 68:327-333. https://doi.org/10.1016/0169-4332(93)90252-7
28. Wang SJ, Tsai HY, Sun S-C (2001) Characterization of sputtered titanium carbide film as

diffusion barrier for copper metallization. Journal of The Electrochemical Society 148:C563-C568. https://doi.org/10.1149/1.1385378

29. Leyendecker T, Rass I, Erkens G, Feldhege M (1997) TiAlN–Al2O3 PVD-multilayer for metal cutting operation. Surface and Coatings Technology 97:790-793. https://doi.org/10.1016/S0257-8972(97)00176-X
30. Wang SQ, Chen L, Yang B, Chang KK, Du Y, Li J, Gang T (2010) Effect of Si addition on microstructure and mechanical properties of Ti–Al–N coating. International Journal of Refractory Metals and Hard Materials 28:593-596. https://doi.org/10.1016/j.ijrmhm.2010.05.001
31. Özgür A, Yalçın B, Koru M (2009) Investigation of the wear performance and thermal diffusivity properties of M41 tools steel coated with various film coatings. Materials & Design 30:414-417. https://doi.org/10.1016/j.matdes.2008.05.020
32. Yen Y-C, Jain A, Chigurupati P, Wu W-T, Altan T (2004) Computer simulation of orthogonal cutting using a tool with multiple coatings. Machining science and technology 8:305-326. https://doi.org/10.1081/mst-200029230
33. Grzesik W, Nieslony P (2004) Physics based modelling of interface temperatures in machining with multilayer coated tools at moderate cutting speeds. International Journal of Machine Tools and Manufacture 44:889-901. https://doi.org/10.1016/j.ijmachtools.2004.02.014
34. Sadat AB, Reddy MY, Wang B (1991) Plastic deformation analysis in machining of Inconel-718 nickel-base superalloy using both experimental and numerical methods. International journal of mechanical sciences 33:829-842. https://doi.org/10.1016/0020-7403(91)90005-N

Figures

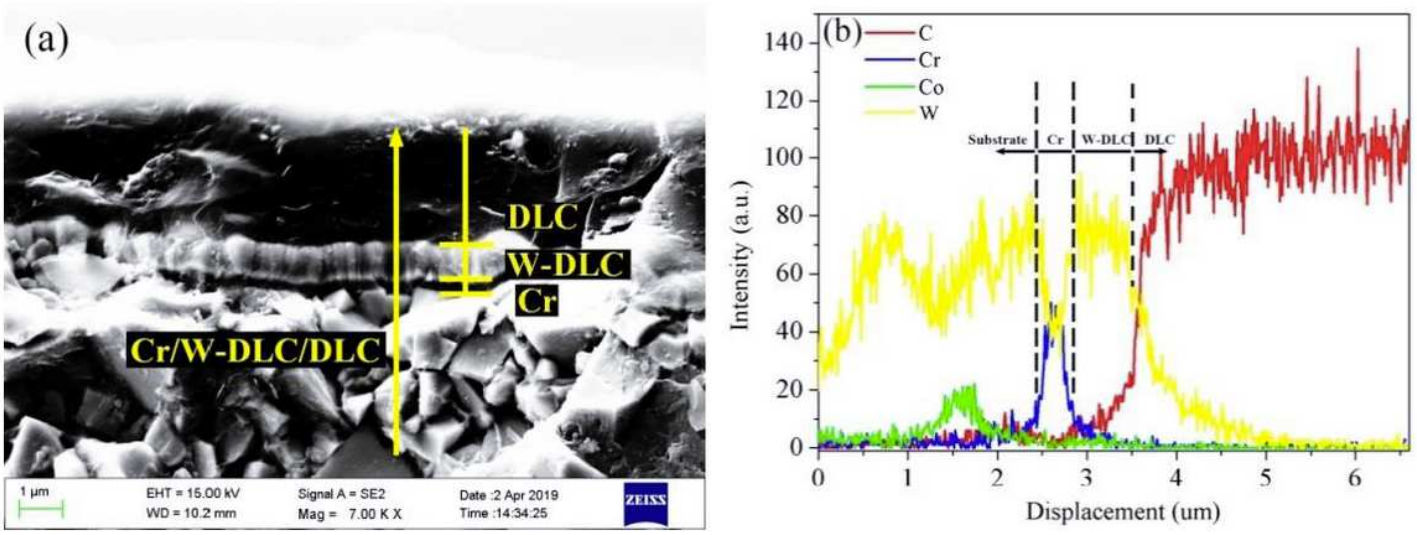

Figure 1

Cross-sectional morphology and element distribution of Cr/W-DLC/DLC coated tools：a：Cross-sectional morphology(b) Cross-sectional element distribution

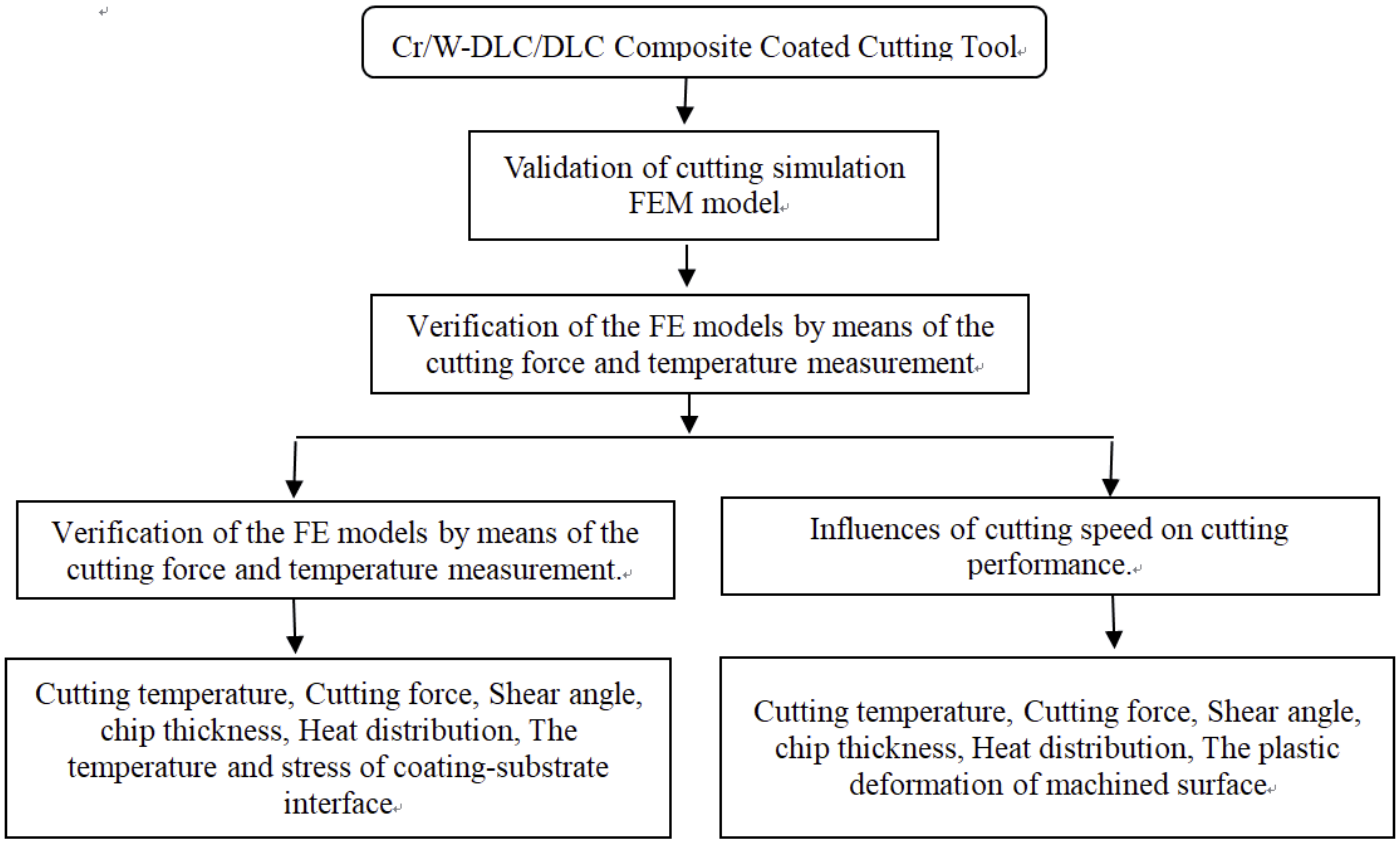

Figure 2

The description of the experiment methodology flow chart

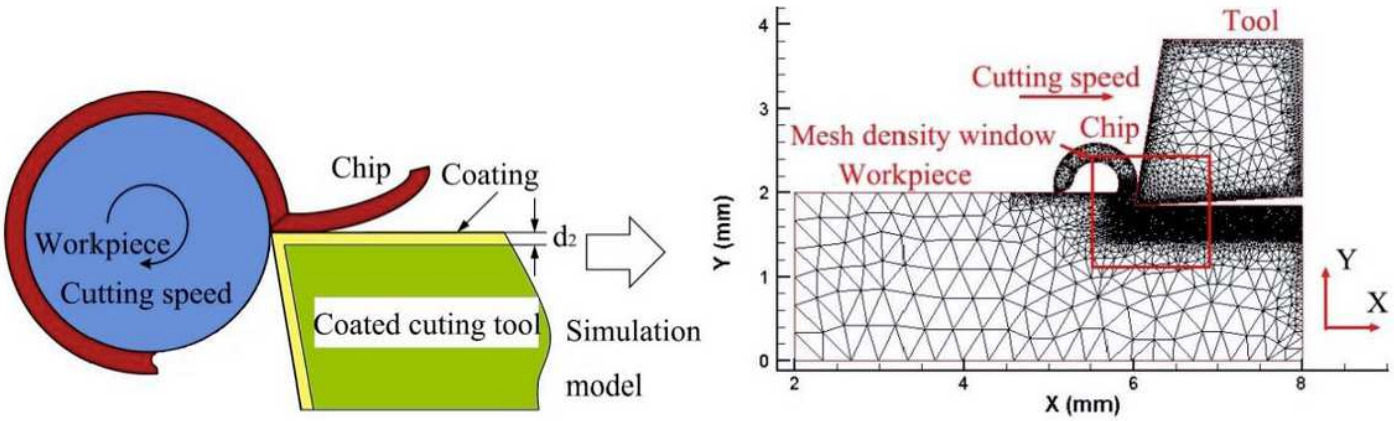

Figure 3

Finite element model of the turning

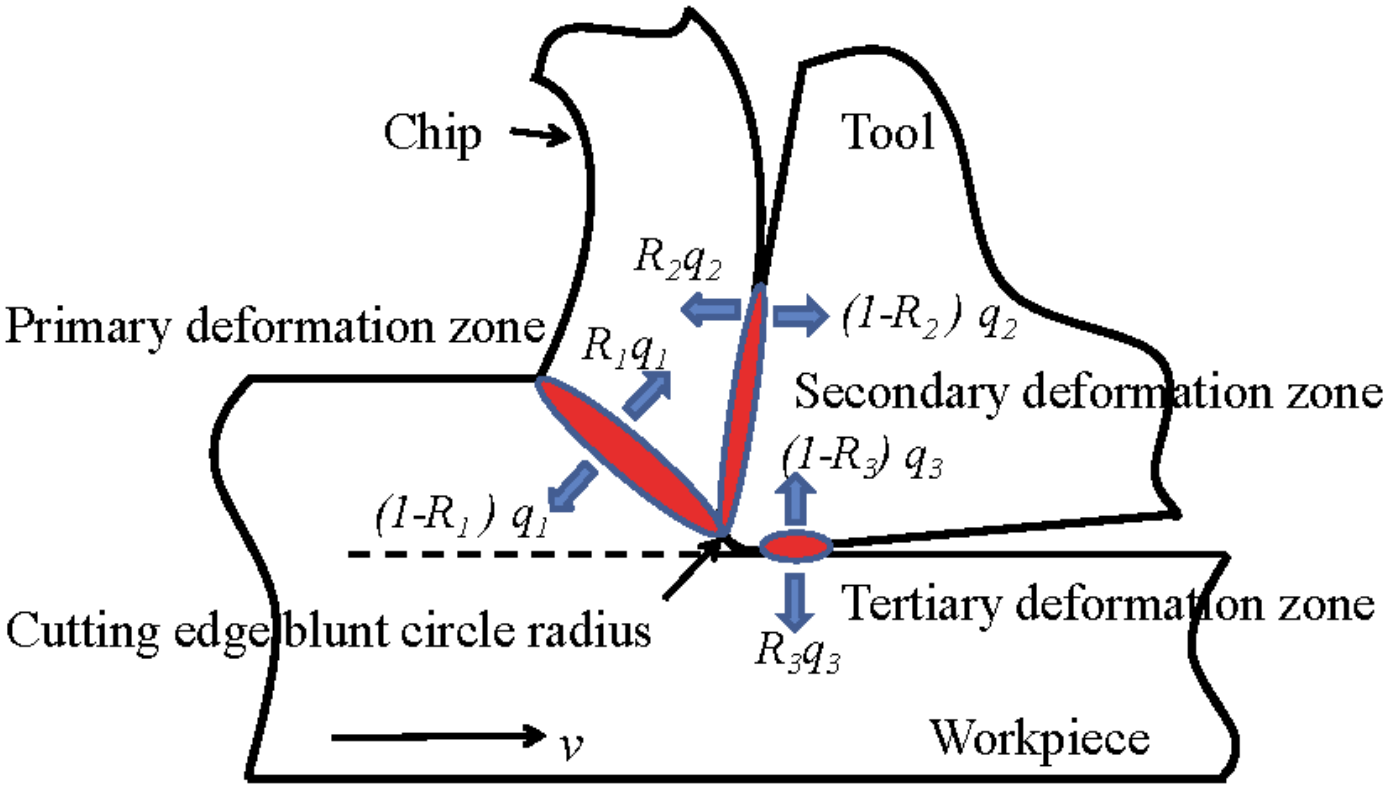

Figure 4

Heat generation and distribution in the cutting deformation zone

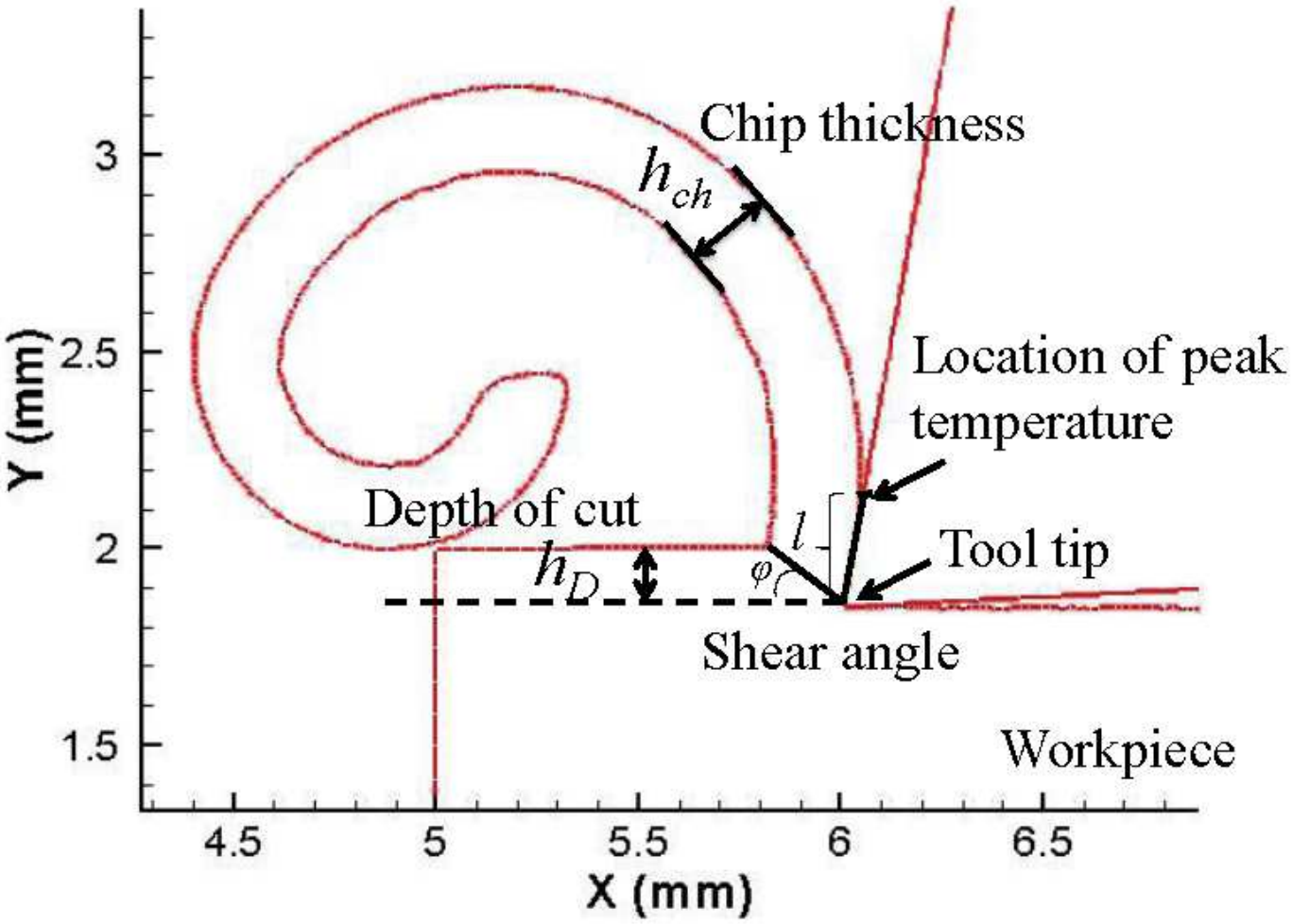

Figure 5

Cutting deformation obtained from FEM simulation

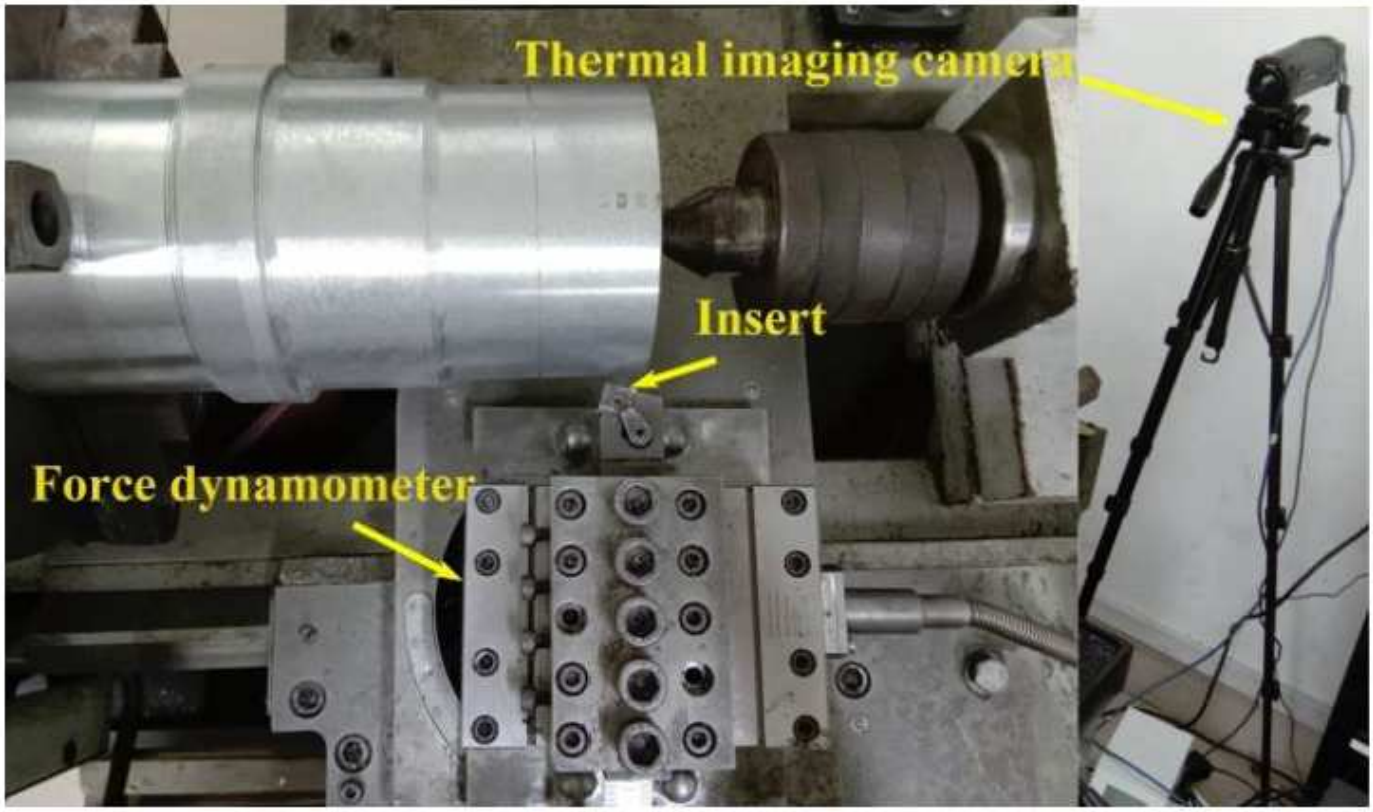

Figure 6

Experimental set up

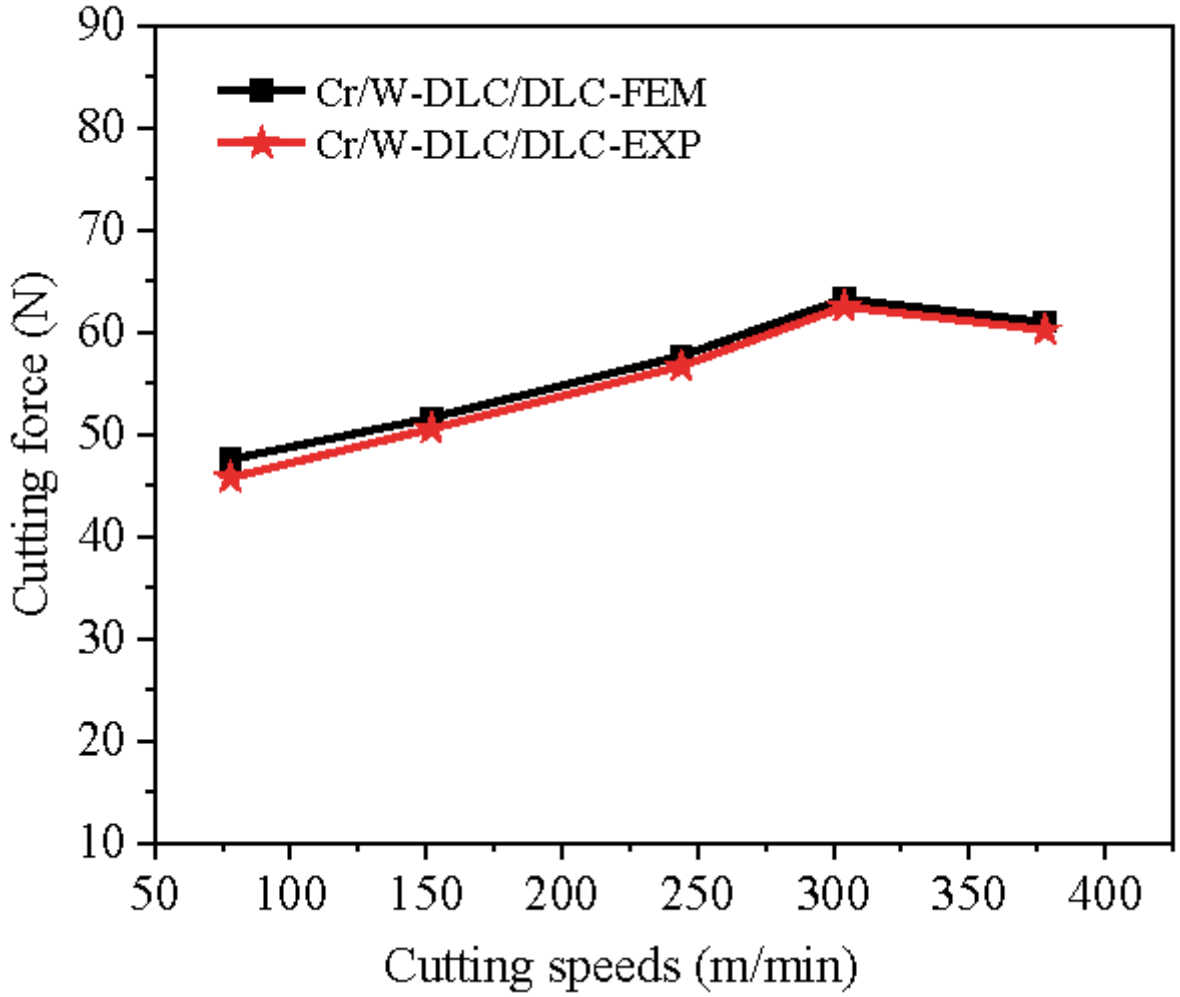

Figure 7

Comparison of the cutting force with experiment and simulation

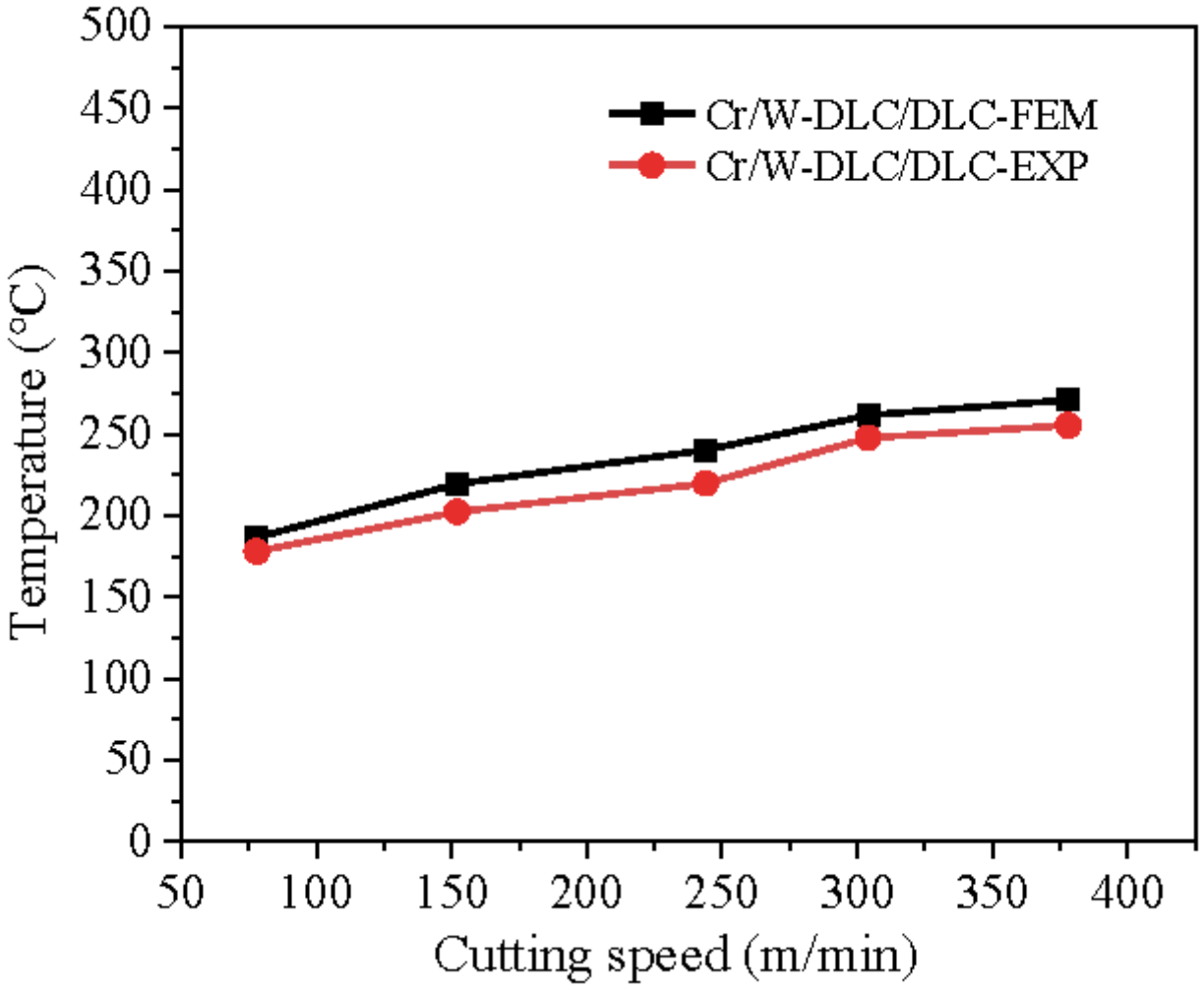

Figure 8

Comparison of the cutting temperature with experiment and simulation

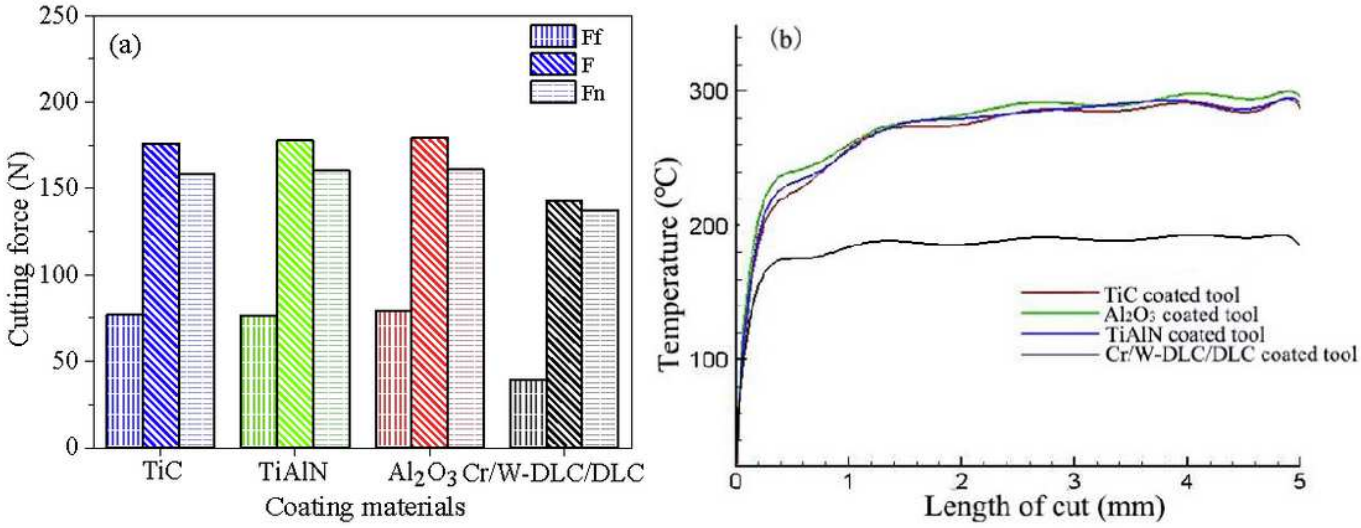

Figure 9

Cutting force and cutting temperature distribution of different coated tools obtained by finite element simulation

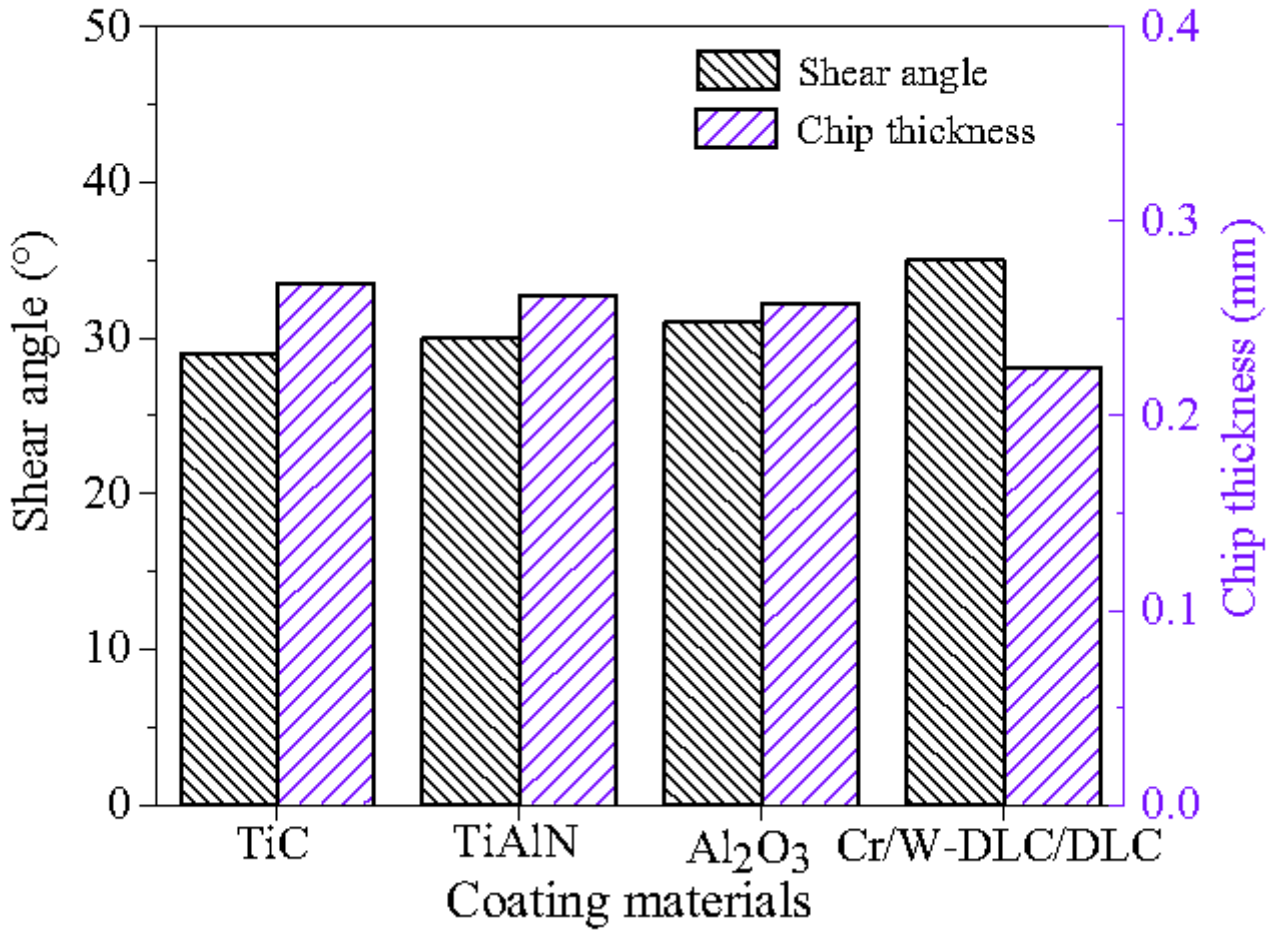

Figure 10

Influence of coating materials on the chip thickness and shear angle

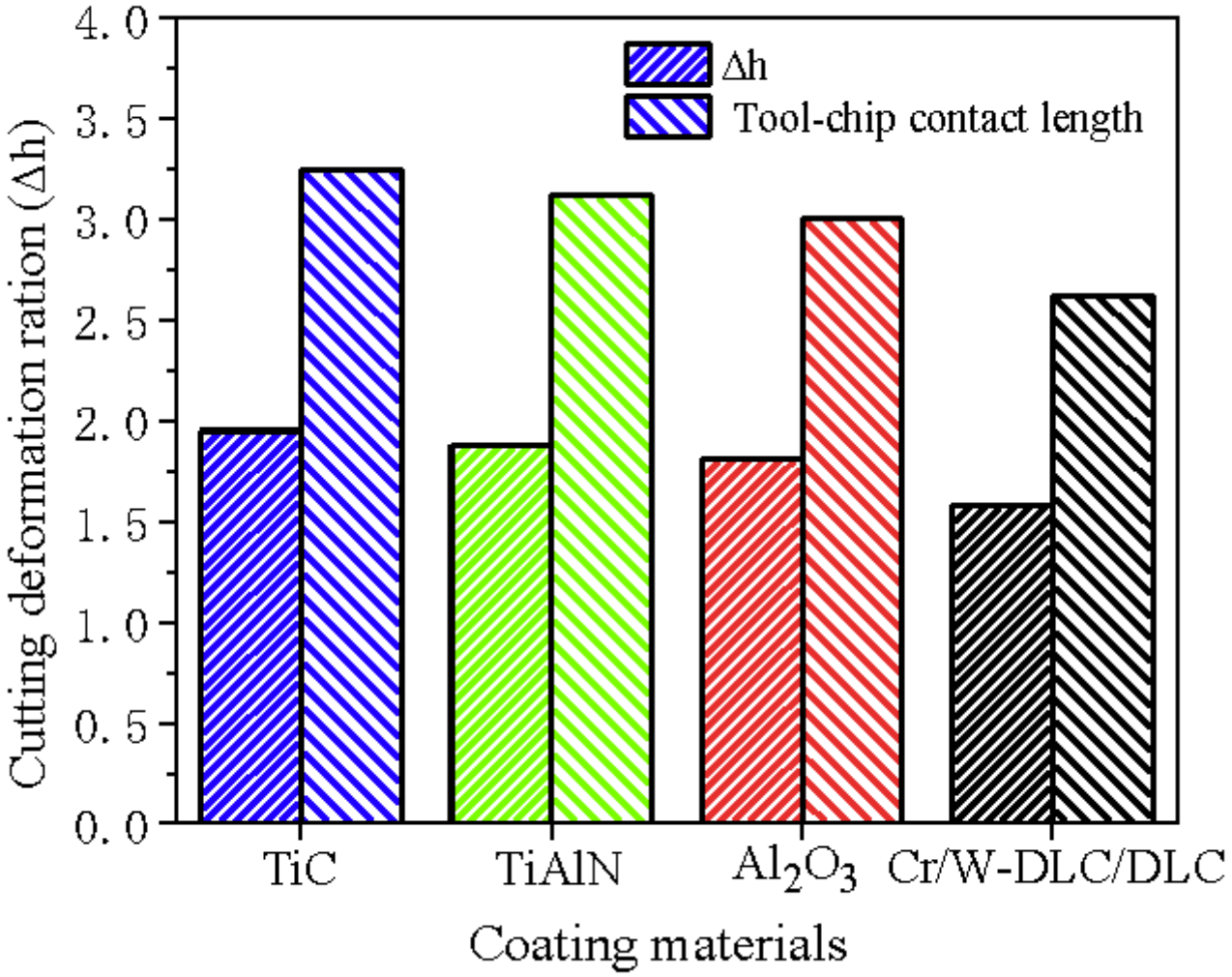

Figure 11

Influence of coating materials on cutting deformation ration and chip contact length

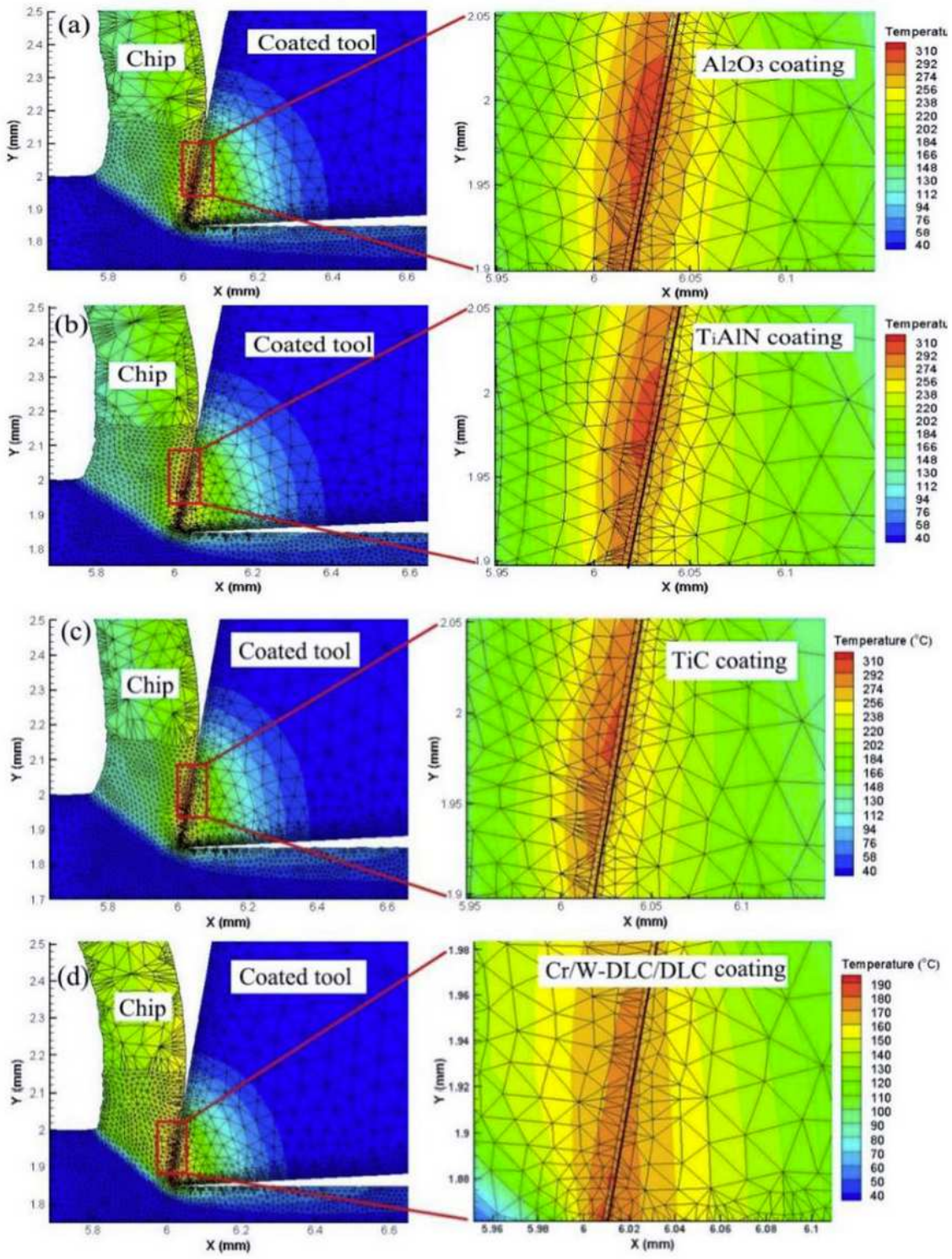

Figure 12

Cutting temperature field of different coated tools (a) Al2O3 coated tools (b) TiAlN coated tools (c) TiC coated tools (d) Cr/W-DLC/DLC coated tools

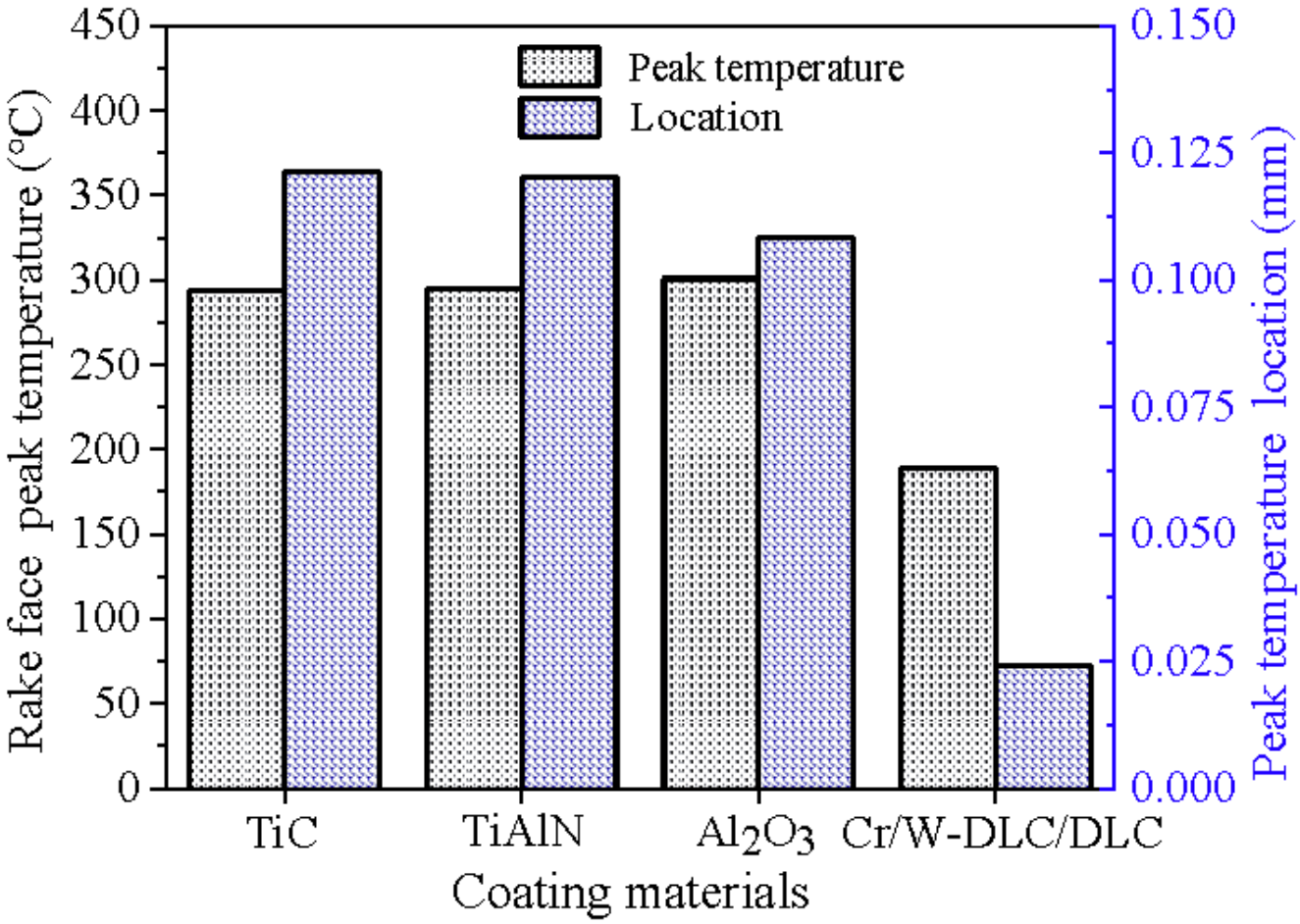

Figure 13

Rake face peak temperature and its location

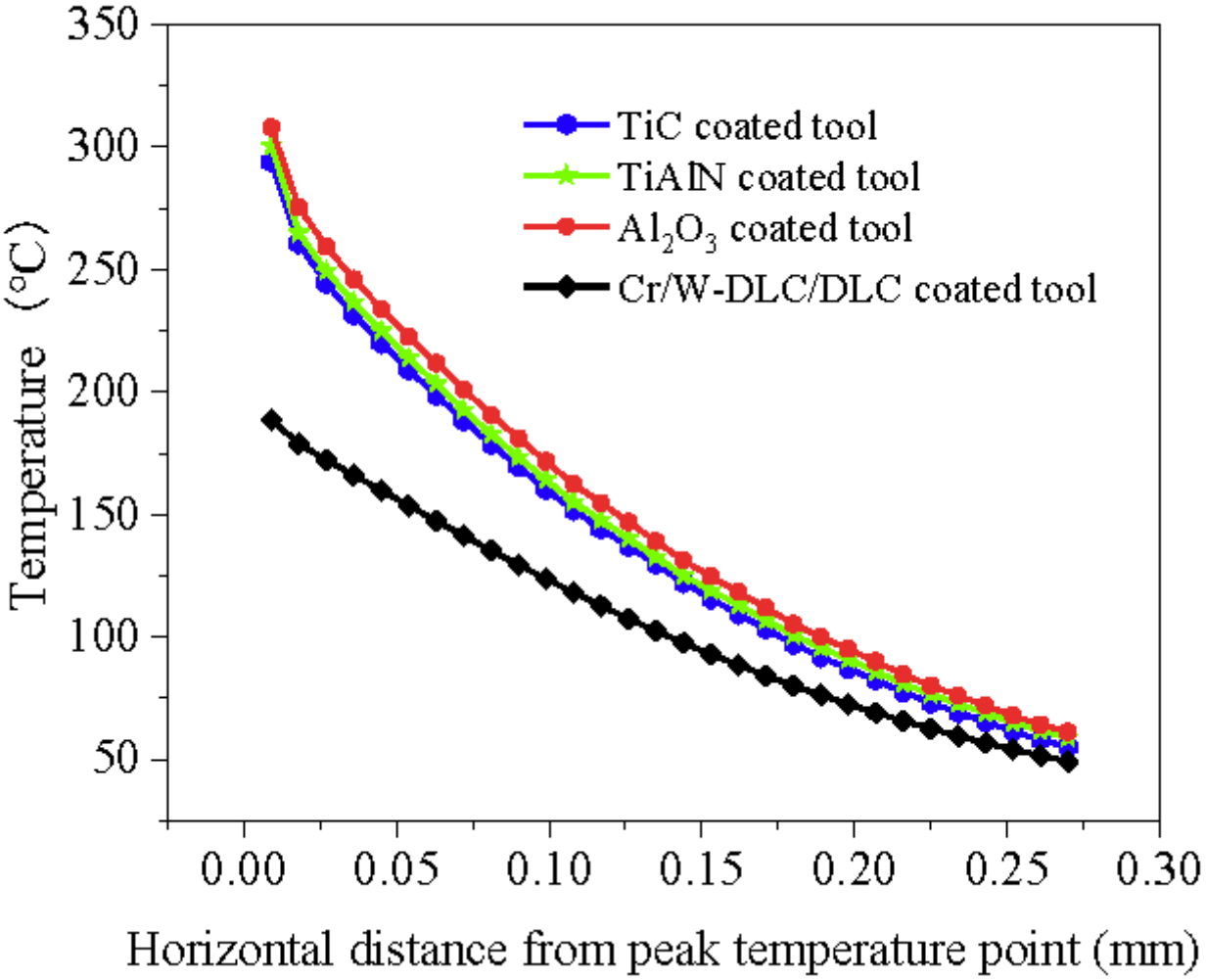

Figure 14

Change of the horizontal distance of the temperature value of the tool with different coatings prolonging the peak temperature of the tool rake face

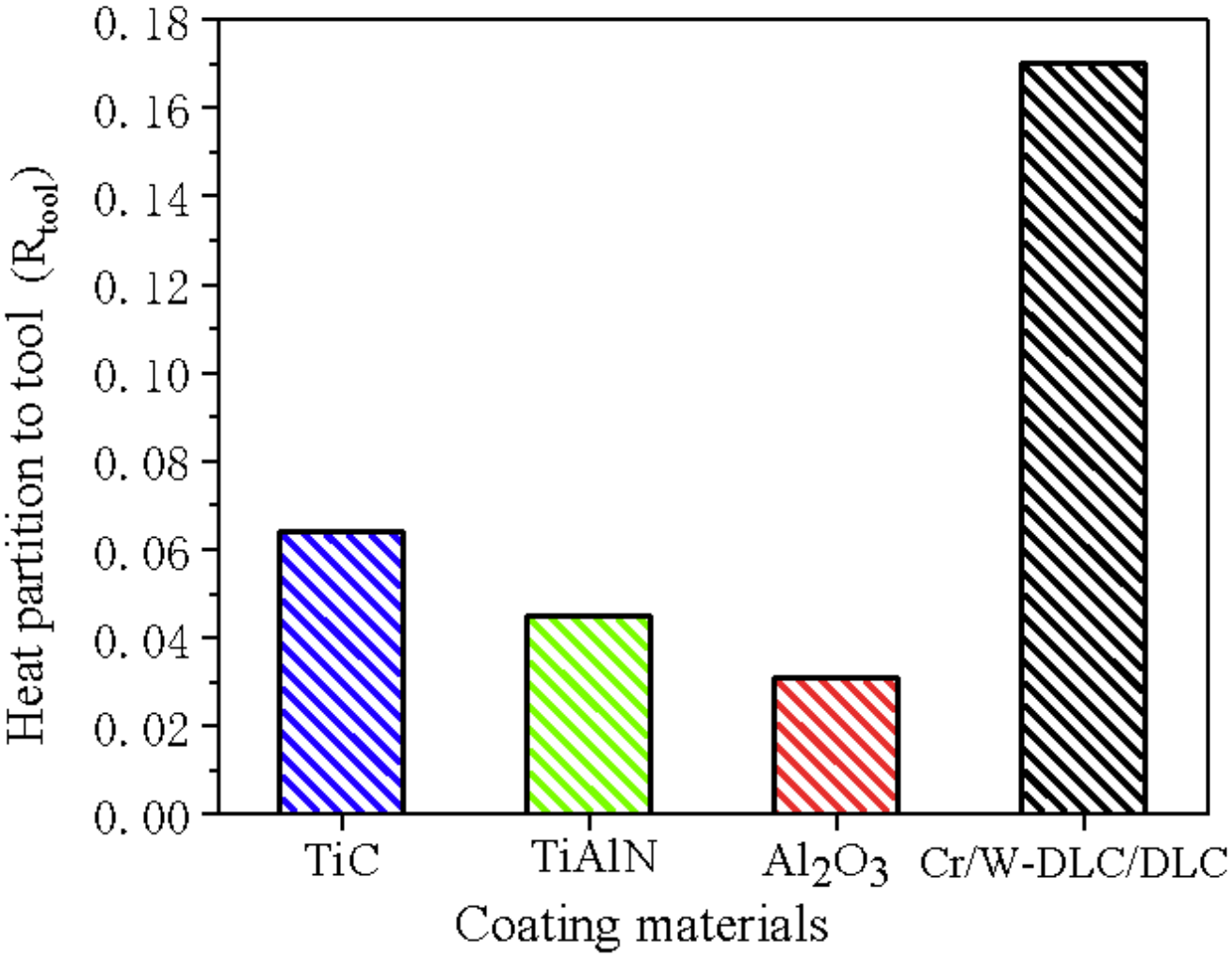

Figure 15

Influence of coating type on the heat partition

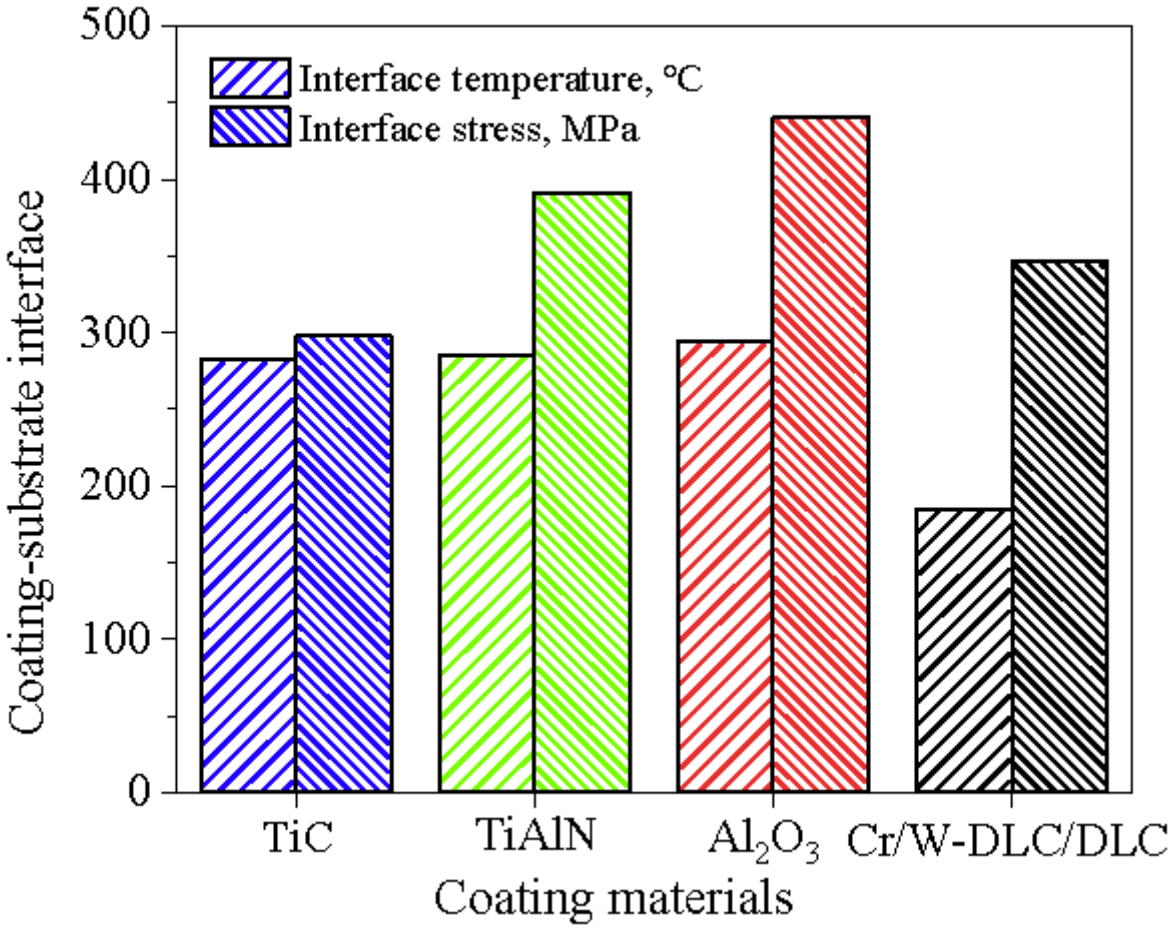

Figure 16

Effect of coating materials on temperature and stress of coating-substrate interface

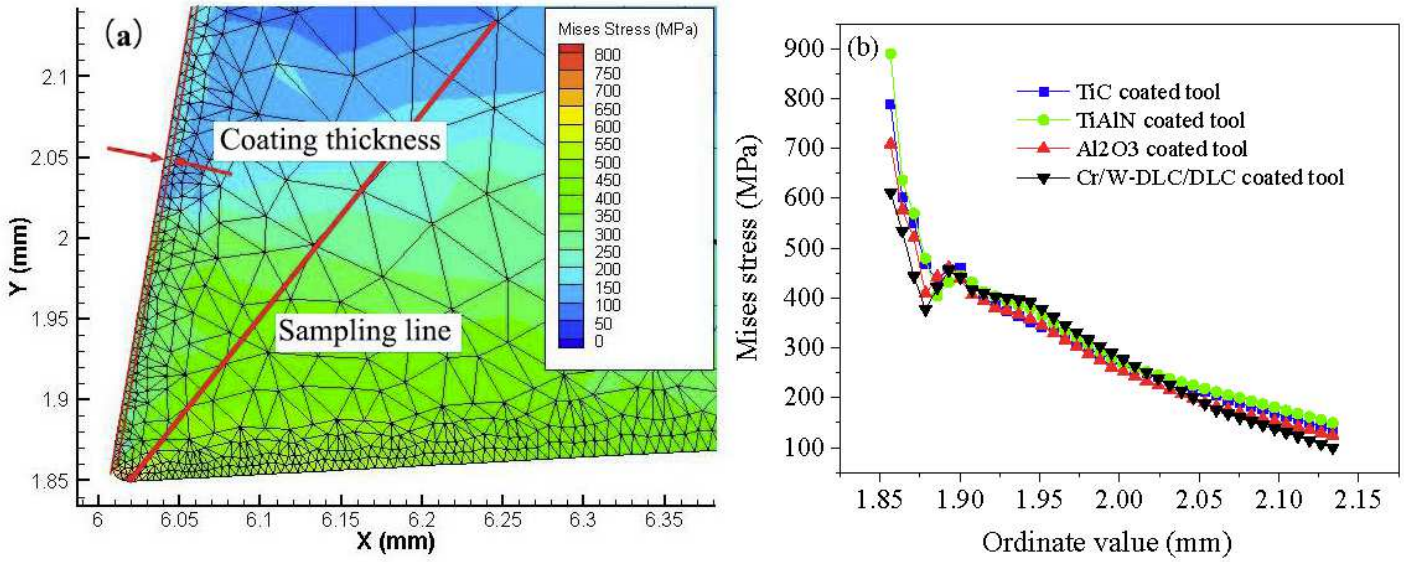

Figure 17

Change in equivalent stress of the tool tip with different coatings

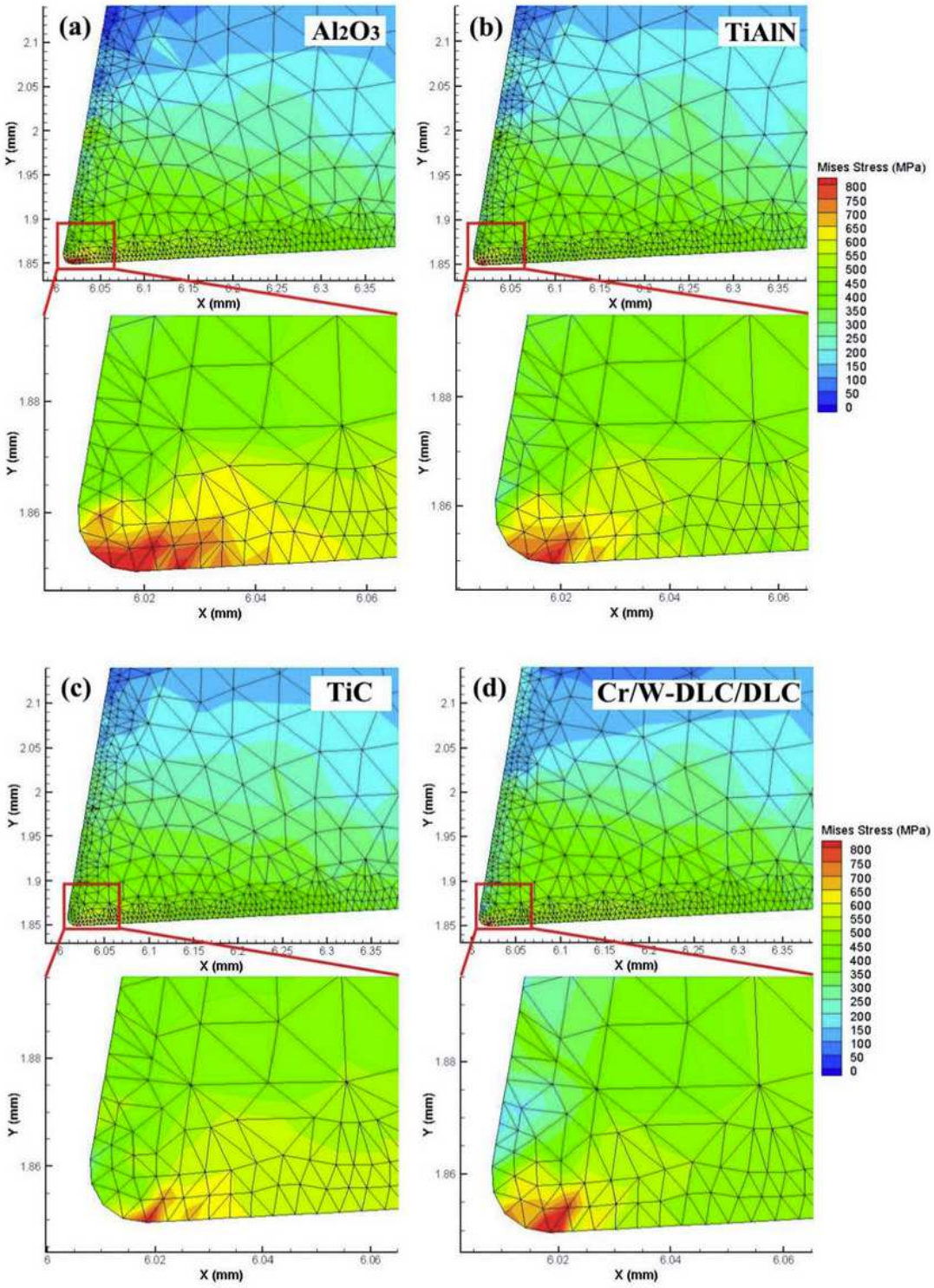

Figure 18

Enlarged equivalent stress of the tool tip of different coated tools

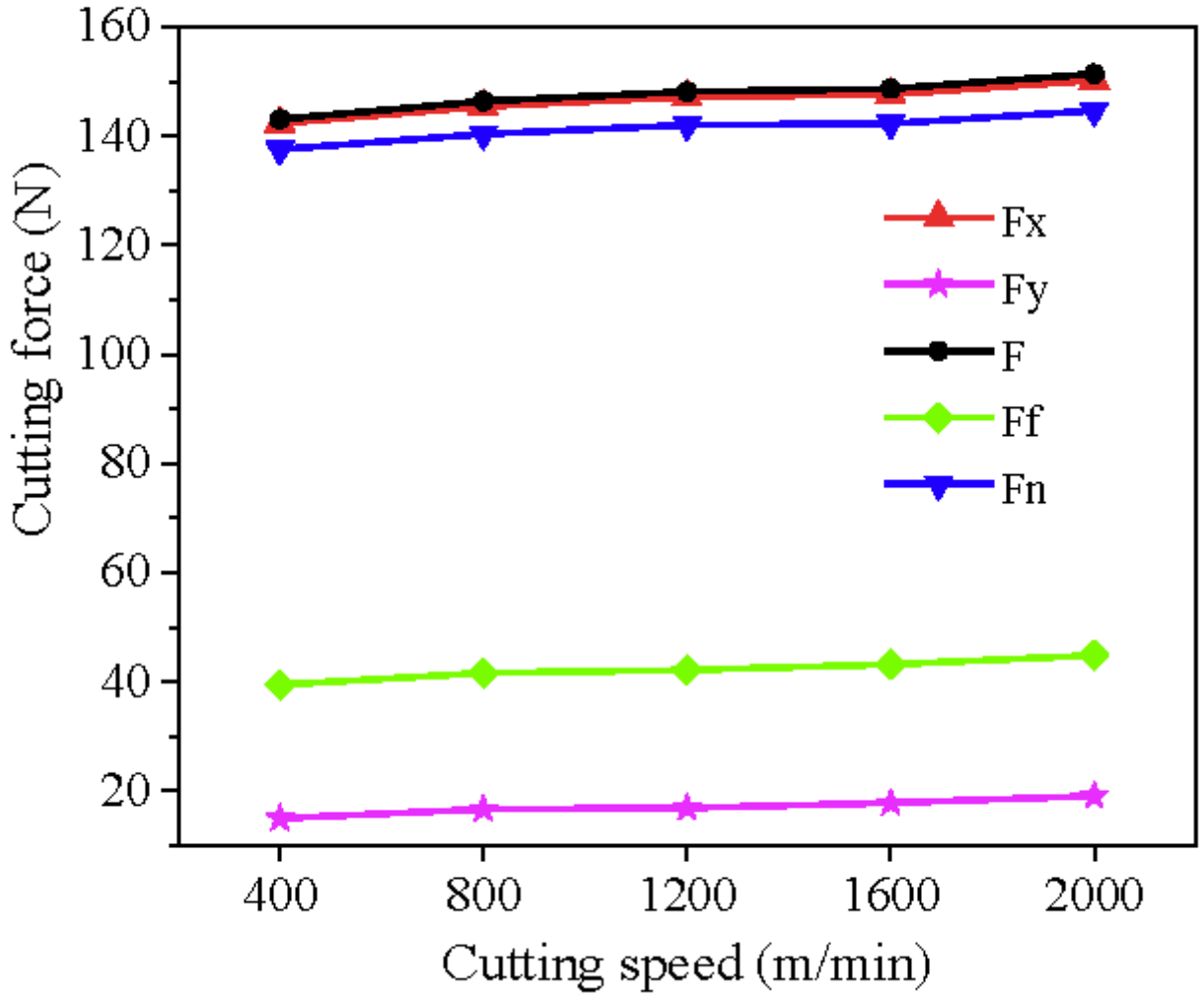

Figure 19

Cutting forces corresponding to different cutting speeds

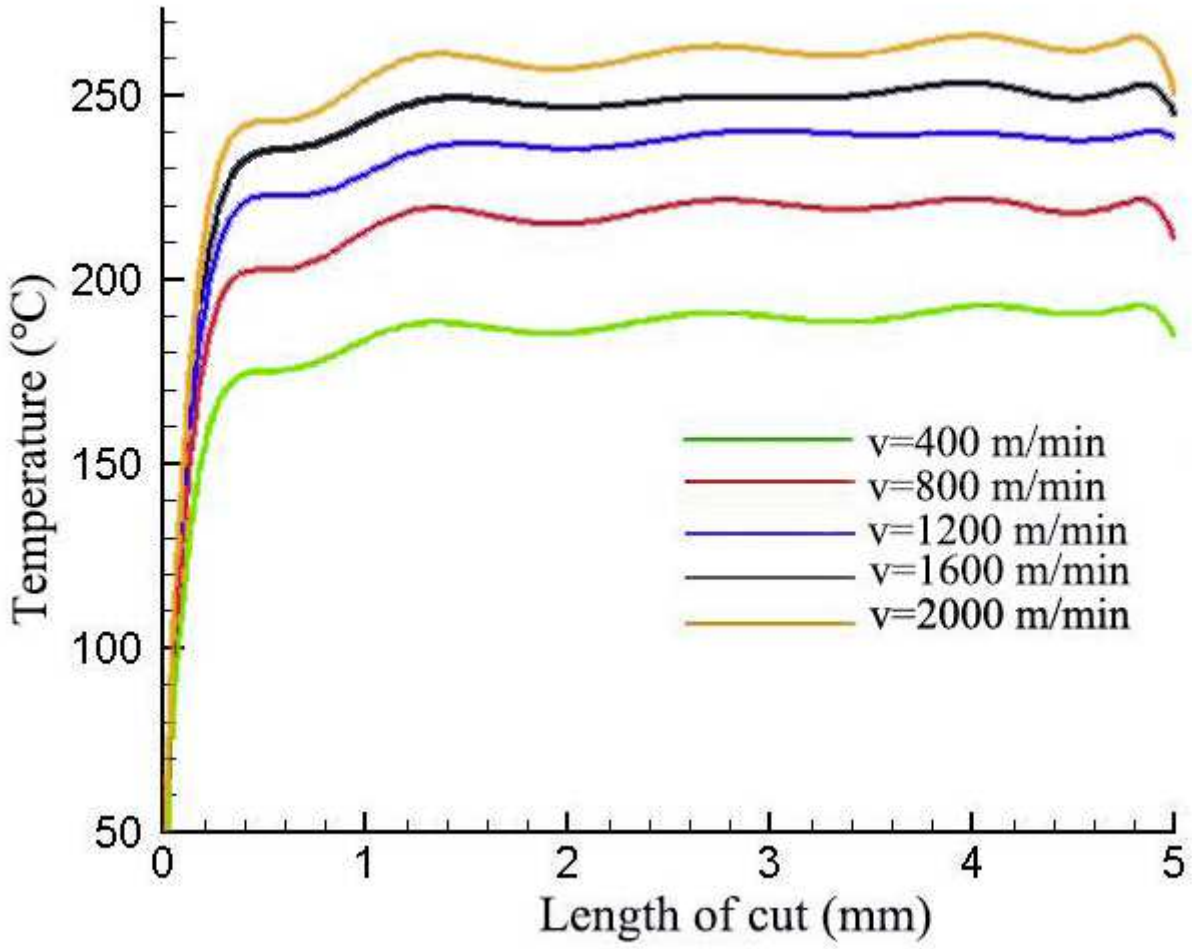

Figure 20

Cutting temperature corresponding to different cutting speeds

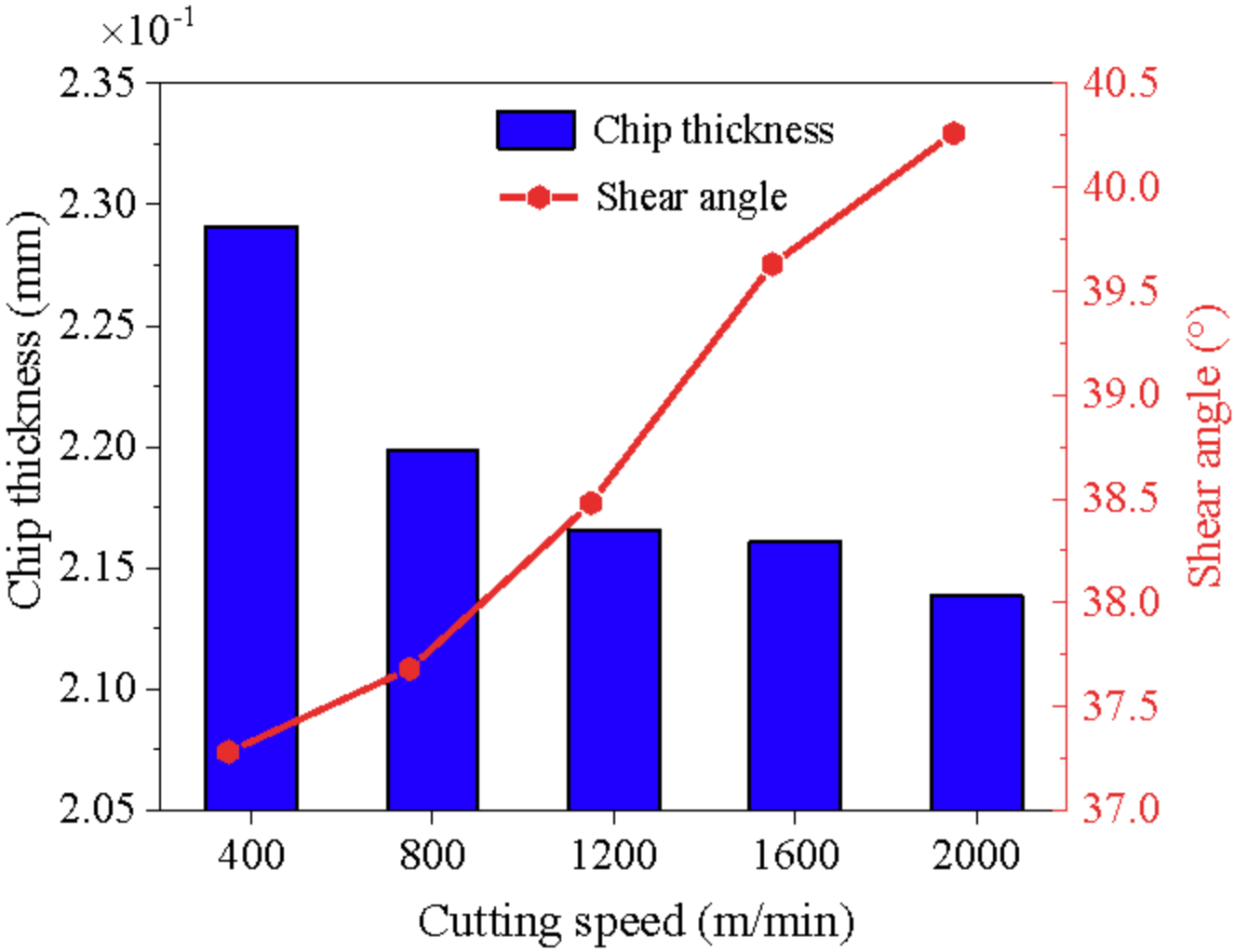

Figure 21

Influence of cutting speeds on shear angle and chip thickness

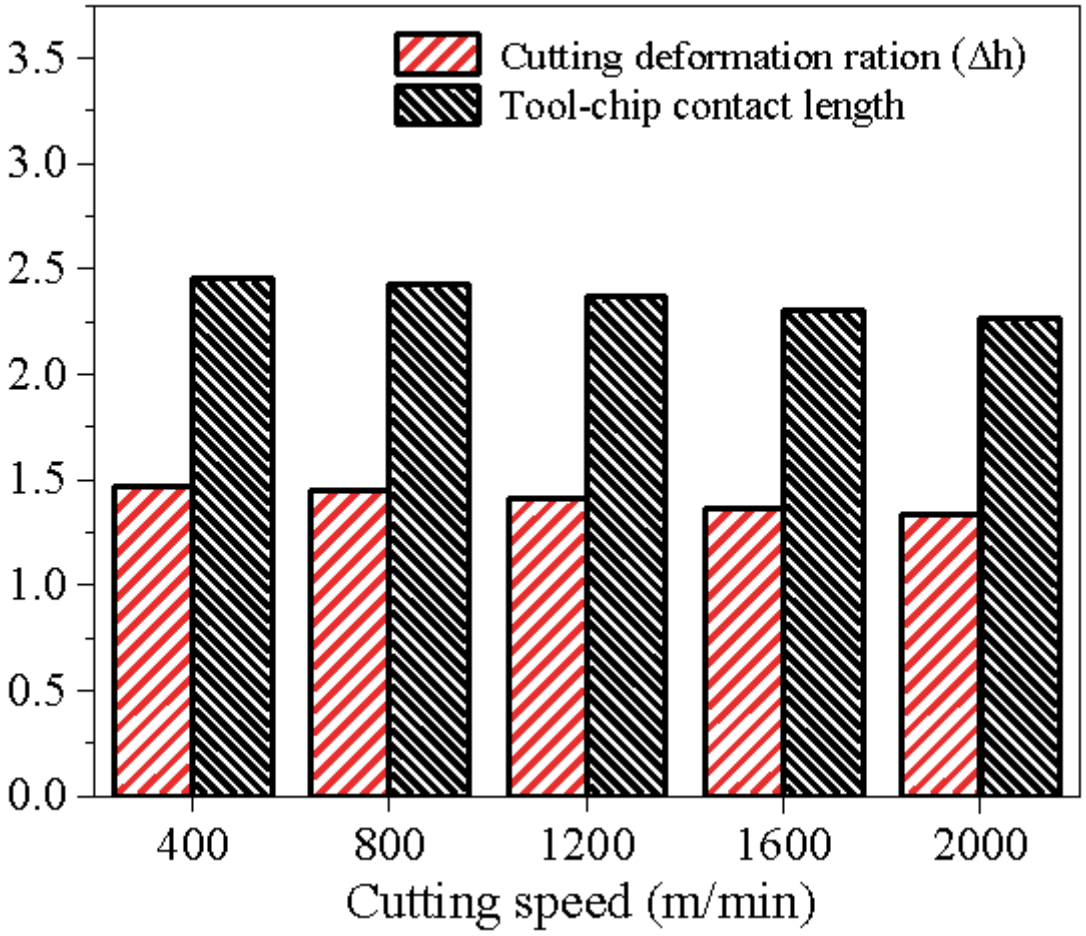

Figure 22

Influence of cutting speed on cutting deformation ration and chip contact length

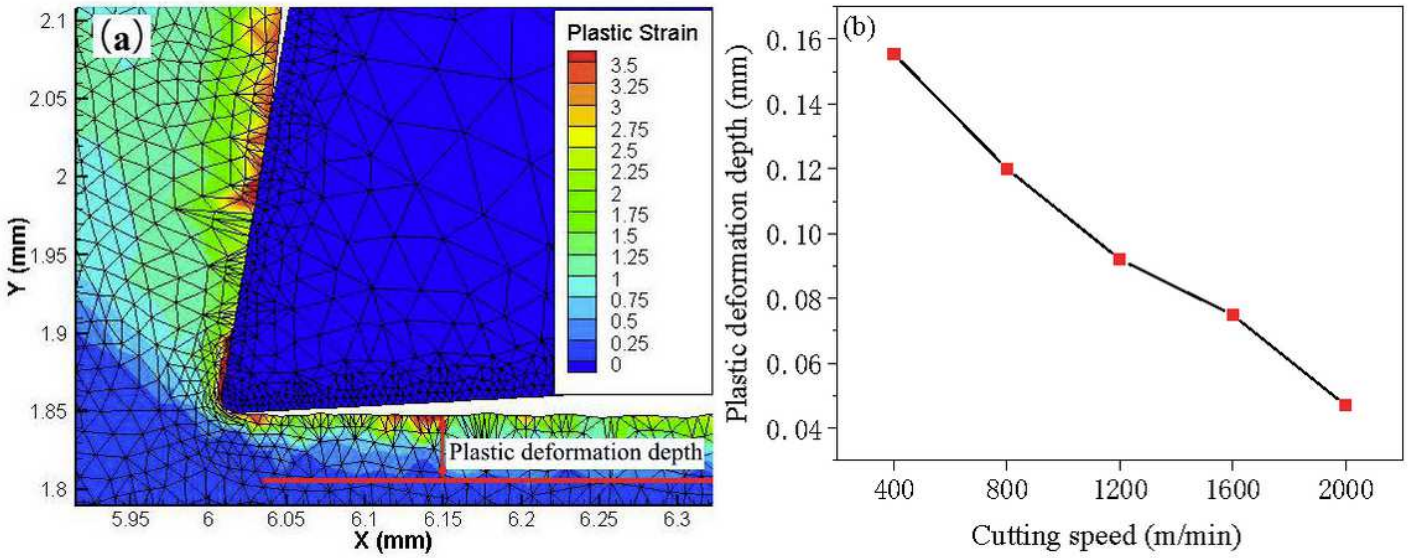

Figure 23

Influence of cutting speed on plastic deformation depth of machined surface

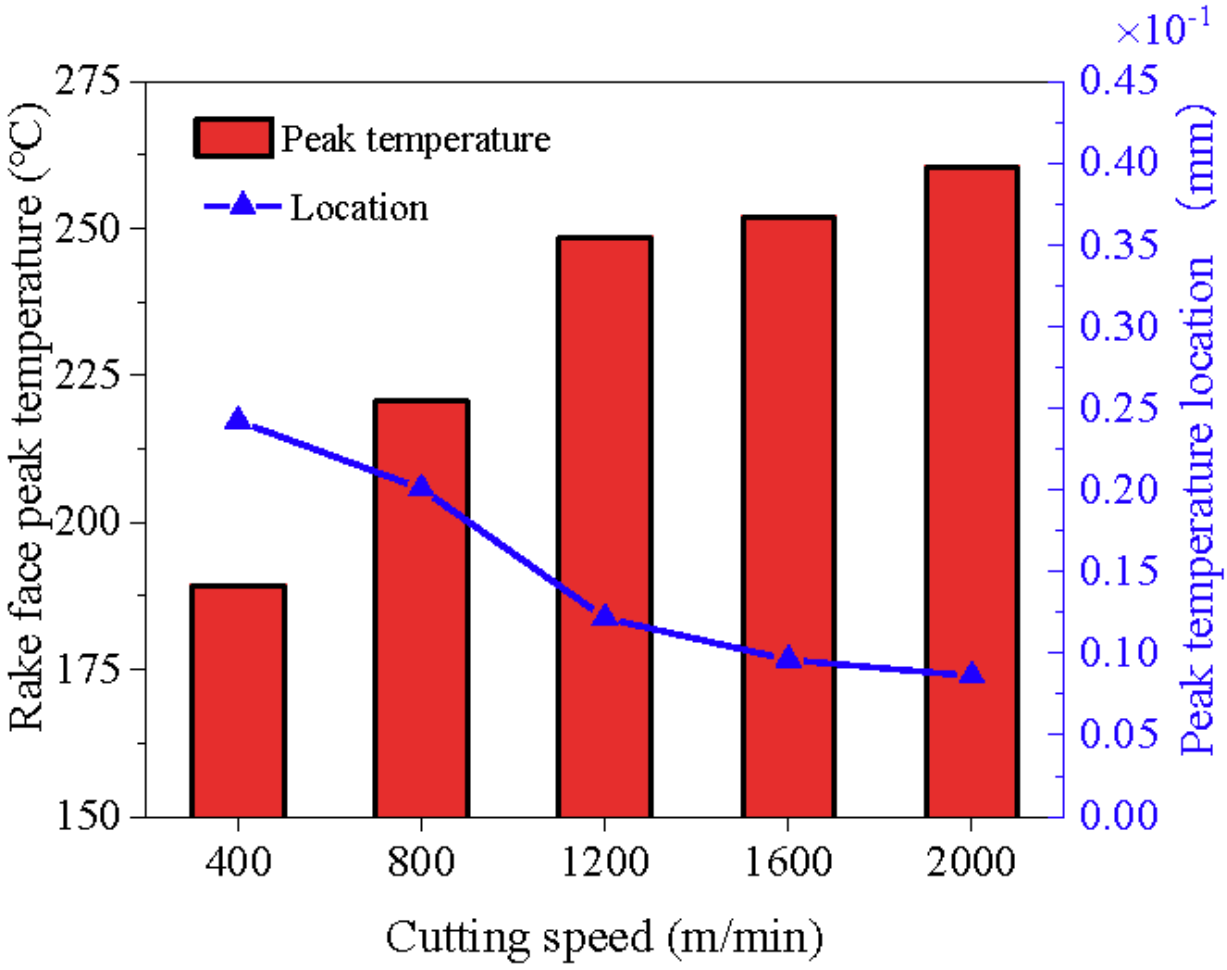

Figure 24

Rake face peak temperature and its location corresponding to different cutting speeds

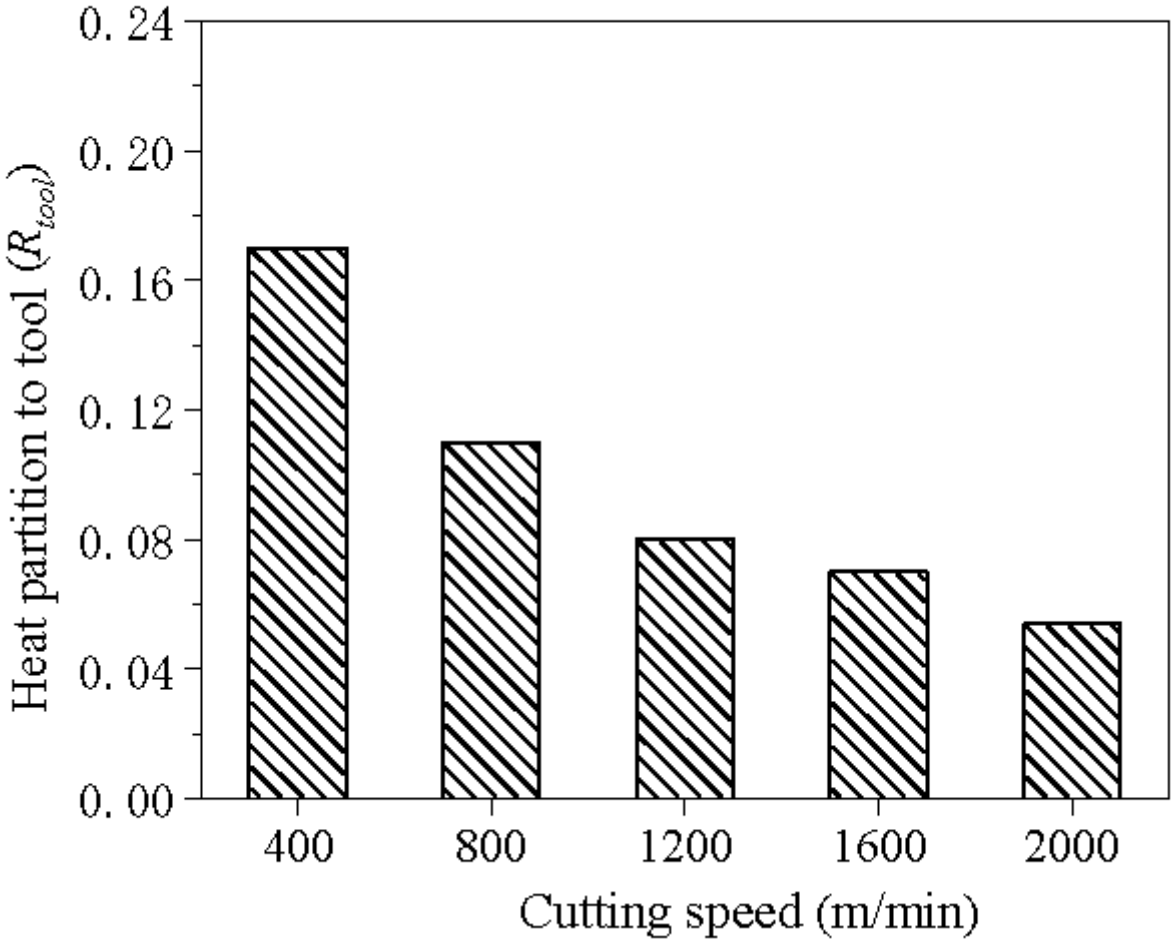

Figure 25

Influence of cutting speeds on the heat partition